Influence of Surface Chemistry on Host/Guest Interactions: A Model Study on Redox-Sensitive β-Cyclodextrin/Ferrocene Complexes

Baptiste Chabaud, Hugues Bonnet, Rémy Lartia, Angéline van der Heyden, Rachel Auzély-Velty, Didier Boturyn, Liliane Coche-Guérente, Galina Dubacheva

Influence of surface chemistry on host/guest interactions: model study on redox-sensitive β-cyclodextrin/ferrocene complexes

Baptiste Chabaud,† Hugues Bonnet,† Rémy Lartia,† Angéline Van Der Heyden,† Rachel Auzély-Velty,⊥ Didier Boturyn,† Liliane Coche-Guérente,† Galina V. Dubacheva†*

† Département de Chimie Moléculaire, Université Grenoble Alpes, CNRS UMR 5250, 570 rue de la chimie, CS 40700, Grenoble 38000, France

⊥CERMAV, Université Grenoble Alpes, CNRS, 38041 Grenoble Cedex 9, France

ABSTRACT: While host/guest interactions are widely used to control molecular assembly on surfaces, quantitative information on the effect of surface chemistry on their efficiency is lacking. To address this question, we combined electrochemical characterization with quartz crystal microbalance with dissipation monitoring to study host/guest interactions between surface-attached ferrocene (Fc) guests and soluble β-cyclodextrin (β-CD) hosts. We identified several parameters which influence the redox response, β-CD complexation ability and repellent properties of Fc monolayers, including the method of Fc grafting, the linker connecting Fc with the surface and the diluting molecule used to tune Fc surface density. The study on monovalent β-CD/Fc complexation was completed by the characterization of multivalent interactions between Fc monolayers and β-CD-functionalized polymers, with new insights being obtained on the interplay between the surface chemistry, binding efficiency and reversibility under electrochemical stimulus. These results should facilitate the design of well-defined functional interfaces and their implementation in stimuli-responsive materials and sensing devices.

1. INTRODUCTION

Controlling molecular assembly on surfaces through host/guest chemistry is a rapidly growing research field with a wide range of approaches developed for the design of nanostructured, stimuli-responsive and biomimetic interfaces.[1–4] A particularly attractive feature of host/guest interactions is the possibility to modulate their binding strength reversibly and on-demand, which can be achieved through a variety of stimuli, including electrochemistry, light, temperature, pH, soluble competitors and their combinations.[4,3,5–7] Combined with multivalent interactions,[2,8–10] stimuli-responsive host/guest complexation allows to design surfaces with advanced properties such as strong binding, on-demand switching, self-sorting and regeneration. Determining the factors which govern these dynamic host/guest interfaces is therefore important for various applications in material sciences (e.g., controlled assembly of molecules/nano-objects,[1–3,5,6,10] patterning,[1–3,5,6] catalysis,[3,11] mechanical actuators[4]), sensing (e.g., small chemicals, biomolecules, cells)[5,6,12,13] and biotechnology (e.g., controlled adhesion of cells/bacteria/viruses,[3,5,6,10] biomimetic (nano-)interfaces[5,9,10,14]).

Despite the wide use of host/guest interactions, our understanding of the parameters determining their efficiency at interfaces, and in particular of the role of the surface chemistry, remains limited. Previous studies highlighted the importance of the parameters related to the host/guest moieties (surface density,[10,15–18] concentration in solution,[17,19] affinity,[17] valency[17,20–25] and lateral mobility),[26] the surrounding liquid medium (presence of competing guests[27,28] or anions[29]) and the underlying substrate (Au, Si, doping level).[30] In particular, it has been shown that the affinity of host/guest complexes is altered at the surface compared to that in solution, with both higher and lower association constants being reported.[18,27,29,31] There are studies suggesting that these effects are related to different chemical structures of guest derivatives, resulting in different combinations of binding forces during the formation of host/guest complexes (hydrophobic, electrostatic, hydrogen bonding).[27,32] Other studies showed that electrolyte anions interact with host cavities with different affinities and, in some cases, interfere with host/guest binding.[18,29] One can expect that the parameters of the interface, including the arrangement of host/guest groups, the linkers connecting them to the surface and the nature of diluting molecules, can also affect the efficiency of host/guest complexation and on-demand dissociation, an aspect that has not yet been studied thoroughly.

To investigate the role of surface chemistry, self-assembled monolayers (SAMs) are among the best candidates, as they are frequently used for implementing host/guest assembly on a surface,[2,5,6,33] while providing versatile platforms to study host/guest interactions with different techniques and in a wide range of experimental conditions. Indeed, SAMs can be formed on various solid supports, including metal/metal oxide, transparent/opaque, conducting/insulating substrates, and combined with different conjugation chemistries to tune their functionality such as acid/amine coupling[34] and click reactions.[16,17,35–38] Moreover, formation of multicomponent SAMs consisting of host/guest derivatives mixed with diluting molecules of interest (e.g., thiols on metal surfaces) allows to tune the

surface density of host/guest groups,[16,17,28,35,38–41] to control their 2D organization[40,41] and to suppress undesired non-specific interactions.[15,16,20,21,42,43] Typically, host/guest assemblies are realized by immobilizing one of the host/guest moieties in SAMs, with the other present in solution in the mono- or multivalent form. More complex architectures composed of different molecules and/or nano-objects have been constructed by alternate deposition of layers containing host and guest moieties.[2,44,45] The possibility to detach SAM adlayers by exposing them to external stimuli such as redox, photo, pH or others, depending on the host/guest nature, has been demonstrated for both mono- and multi-layered systems.[2,3,5–7,11,44] For all these different architectures, understanding the correlations between the interfacial properties of SAMs and the resulting host/guest interactions is critical for achieving both efficient assembly and on-demand detachment.

To perform such study, we chose as a model system host/guest interactions between cyclodextrins and their hydrophobic guests. Cyclodextrins belong to the class of naturally occurring receptors, which are cyclic glucopyranose oligomers of toroidal shape. Cyclodextrins have an affinity for hydrophobic molecules in their inner cavity, while their outer surface is hydrophilic. The choice of cyclodextrins was motivated by several reasons. First of all, their stimuli-responsive complexes are widely used to design tunable and/or dynamic functional surfaces.[2,5,46] In addition, numerous synthetic strategies have been developed to graft cyclodextrins and their guests to inorganic, organic and biomolecular scaffolds.[33,47,48] This, combined with well-established surface chemistries (e.g., thiol, silane, diazonium, lipid bilayers[33,39,46]) and the possibility to use different stimuli (e.g., electrochemistry[15,22,34,35,42–44] or light[49–54]), made cyclodextrin/guest chemistry a powerful tool to control surface binding of various molecules and nano-objects from linear polymers[35] and dendrimers[2,44] to nanoparticles,[44] proteins,[5,22,42,49] cells[5,15,34,43,52,53] and pathogens.[5,50,51] Furthermore, the solubility of cyclodextrin complexes at physiological conditions and their wide affinity range (K_d = 0.01 - 100 mM[55]) allowed their use for mimicking and studying biological interactions at functional interfaces.[46]

Similar to other host/guest systems, SAMs composed of cyclodextrins or their guests are commonly used to apply cyclodextrin chemistry at interfaces, with the most ubiquitous being thiolated derivatives immobilized on gold surfaces. Indeed, most studies on cyclodextrin monolayers are performed on gold surfaces,[2,25,27,29,35,56–59] but also on other types of substrates such as silicon, silicon oxide and mica.[19,30,52,53] Studies on thiolated monolayers highlighted the dependence of cyclodextrin orientation on the number of thiol ligations made between the cyclodextrin cavity and the metal surface.[58,59] Guest SAMs can be formed through different chemistries, including thiol, silane and diazonium, with the most common substrates being gold and, to a lesser extent, silicon and silicon oxide.[5,11,33,39] In addition to the direct formation of SAMs, i.e., using surface-interacting derivatives of cyclodextrins or their guests, a two-step approach based on the formation of reactive SAMs followed by their post-functionalization with cyclodextrins/guests (e.g., *via* acid/amine or click reactions) has been introduced.[16,35,37,38,60] This two-step protocol was shown to be efficient for the design of tunable surfaces with quantitative control of the density and affinity of surface binding sites.[16,17,35,38] Whether direct grafting or post-functionalization, the use of diluting molecules was shown to be crucial for achieving desired SAM properties, including tunable cyclodextrin/guest surface density,[16–18,35,38,40,41,61] homogeneous distribution of cyclodextrin/guest groups in the monolayer[40,41,61] and suppressed nonspecific interactions.[16,34,35,42,43] Based on these studies, we included the method of SAM formation and the type of diluting molecule in the list of tunable parameters and selected ferrocene (Fc) SAMs on gold as a model system to study their effect on host/guest interactions.

Using redox-active guests such as Fc enables advanced electrochemical characterization of guest SAMs, namely the evaluation of the areal density and 2D organization of guest moieties. Thus, the presence of several guest populations has been revealed in the Fc SAMs, which are directly formed on gold surfaces, reflected by multiple redox peaks in cyclic voltammograms (CVs), the latter being interpreted as isolated and clustered guest moieties.[40,41,61–63] This heterogeneity was associated with several parameters, including surface roughness,[62] SAM properties (Fc linkers, Fc density, Fc packing, diluents)[40,41,62] and liquid phase composition (solvent, present anions, added molecules).[61–64] Furthermore, studies on Fc SAMs reveal a complex interplay between their 2D organization, charge transfer efficiency and interfacial characteristics such as the linker connecting Fc to the surface, Fc surface density and the diluting thiol used to tune Fc surface density.[18,40,60,65,66] Typically, one of these parameters, e.g. the length of the Fc linker,[60,65] is tuned and its effect on Fc organization and/or charge transfer is studied. An extensive study, in which the effects of different interfacial parameters are compared under the same conditions (i.e., same surface, same host/guest derivatives, same electrolyte) is missing. More importantly, the number of studies on the effect of these parameters on the resulting host/guest interactions is very limited.[18,67] In addition, not only the length and fraction of the host/guest linkers and diluents, but also their nature (hydrophilicity, flexibility) may affect host/guest assembly by changing the strength of host/guest complexation and/or non-specific interactions. This complexity raises the important question of the relationship between the chosen surface chemistry, the expected characteristics of the host/guest interfaces, and the efficiency of the resulting host/guest interactions.

Here, we addressed this question by analyzing the interaction of β-CDs with Fc-displaying SAMs while varying several interfacial parameters systematically (i.e., one parameter at a time). We compared direct formation of Fc SAMs through self-assembly of Fc-terminated thiols with a two-step procedure involving the formation of azide-terminated SAMs and their post-functionalization with Fc-alkyne through click reaction. We examined the role of the linker that connects Fc to the gold surface and of the diluting thiol used to adjust the surface density of Fc. The results obtained for free β-CD in solution were completed by the study of Fc SAM interaction with multivalent β-CD scaffolds. This study highlights the importance of surface chemistry in host/guest interactions and demonstrates how this can be

exploited for the rational design of stimuli-responsive interfaces.

2. EXPERIMENTAL SECTION

Materials. HS-$(CH_2)_{11}$-EG_6-N_3 (EG - ethylene glycol), HS-$(CH_2)_{11}$-EG_4-OH, HS-$(CH_2)_{11}$-Fc (Fc - ferrocene, Fig. 2) and HS-$(CH_2)_{11}$-N_3 were purchased from Prochimia. HS-EG_n-N_3 (600 g/mol) and HS-EG_n-CH_3 (350 g/mol) were purchased from Nanocs. HS-$(CH_2)_{10}$-CH_3, (tris[(1-benzyl-1H-1,2,3-triazol-4-yl)-methylamine (TBTA), sodium-L-ascorbate, copper sulfate, ethynylferrocene (Fig. 2), β-CD, 1-adamantanecarboxylic acid (AD-COOH), bovine serum albumin (BSA) and other chemicals were purchased from Sigma-Aldrich-Fluka. HA-β-CD was synthesized by grafting β-CD onto hyaluronic acid (HA, 20 kg/mol, Lifecore Biomedical) *via* esterification of HA hydroxyl groups with pentenoic anhydride, followed by reaction with the thiol derivative of β-CD as described previously.[16] The degree of substitution, $DS_{\beta\text{-CD}}$ = 13% (i.e., the fraction of disaccharides functionalized with β-CD), was determined by integrating the NMR signals arising from the HA and β-CD protons.[16] From the M_w of HA and the $DS_{\beta\text{-CD}}$, the average molecular weight of the modified polymer (M_w of HA-β-CD), the average distance between β-CDs along the contour of the polymer chain, and the average number of β-CDs per polymer chain ($n_{\beta\text{-CD}}$) were calculated to be 26 kg/mol, 7 nm and 7, respectively. The water used in all experiments was purified to achieve a resistivity of 18.2 MΩ cm. Gold-coated QCM-D sensors with a 4.95 MHz resonance frequency were purchased from Quantum Design S.A.R.L. (Biolin Scientific).

SAM formation and click reaction. SAMs were formed using the protocol described previously.[35] Briefly, gold surfaces were rinsed with water and dried with nitrogen, followed by a UV-ozone treatment for 10 min. After that, the surfaces were immersed in ethanol solutions containing one or several thiols (1 mM total concentration). The next day, the functionalized surfaces were thoroughly rinsed with ethanol and dried with nitrogen. Fc grafting to the preformed N_3-terminated SAMs was done through click reaction *via* Cu(I)-catalyzed alkyne azide cycloaddition.[68] The previously established protocol involved *in situ* generation of Cu(I) stabilized by TBTA in t-butanol/water mixture.[35] Briefly, 30 μL of 20 mM aqueous $CuSO_4$ solution was first added to 200 μL of t-butanol solution containing 3 mM TBTA, followed by the addition of 170 μL of 25 mM aqueous solution of sodium-L-ascorbate and 200 μL of 3 mM t-butanol solution of ethynylferrocene. N_3-terminated SAMs were incubated for at least 2 hours in the resulting mixture. Then, the functionalized surfaces were rinsed with t-butanol:water (2:1) mixture and water. The obtained Fc-terminated SAMs were characterized by cyclic voltammetry, contact angle and QCM-D measurements the same day.

Electrochemistry. Electrochemical experiments were performed with a three-electrode potentiostatic system (CHI 440 potentiostat, CH-Instruments, Inc.). Electrode potentials were measured with reference to Ag/AgCl, KCl (3 M). The counter electrode was platinum, and the working electrode was the gold sensor functionalized as described above. The electrochemical cell was home-made, with the working electrode being at the base covered with the electrolyte solution in which the counter and reference electrodes were immersed. The electrolyte solution was 0.1 M aqueous solution of KPF_6. Cyclic voltammograms (CVs) were recorded at the scan rate of 0.1 V/s. The surface density of ferrocene (Fc) molecules (Γ_{Fc}) was calculated from an anodic peak using Faraday's equation:

$$\Gamma_{Fc} = \frac{Q}{F \cdot z \cdot A} \quad (1)$$

where Q is the electric charge transferred through the electroactive layer (C), F is the Faraday constant (96485 C/mol), z is the number of electrons transferred per molecule ($z_{Fc/Fc+}$ = 1) and A is the surface area of the electrode (A = 1.01 cm^2 as previously determined[35]). The formal potentials were estimated from the mean of the oxidation and reduction peak potentials, E_{pa} and E_{pc}, as: $E^{0\prime} = (E_{pa} + E_{pc})/2$. The peak-to-peak splitting was calculated as $\Delta E_p = E_{pa} - E_{pc}$.

Quartz crystal microbalance with dissipation monitoring (QCM-D). QCM-D measurements were performed using QCM-D D300 one chamber system (Q-Sense, Sweden). Resonance frequency (f) and dissipation (D), were recorded at 24 °C for the fundamental resonance as well as for the other overtones (n = 3, 5, 7, 9, 11, 13). A combination of electrochemical and QCM-D measurements (E-QCM-D) was performed using the electrochemical QCM-D module (Q-Sense, Sweden) connected to a CHI 440 potentiostat (CH-Instruments, Inc.) as described above. Electrode potentials were measured with reference to Ag/AgCl, KCl (3 M). The counter electrode was platinum, and the working electrode was the gold sensor. The working electrode mounted in an electrochemical QCM-D module was covered with the electrolyte solution in which the counter and the reference electrodes were immersed. The flow rate during QCM-D measurements was 20-50 μL/min, while flow was stopped during recording CVs. The mass of the attached host probe, including the solvent molecules ($\Gamma^{\text{hydrated}}_{\text{host probe}}$), was determined by fitting QCM-D data to a continuum viscoelastic model implemented in the software QTM (D. Johannsmann, Technical University of Clausthal, Germany). Viscoelastic properties were parameterized in terms of the shear storage modulus $G'(f)$ and the shear loss modulus $G''(f)$. Their frequency dependencies were assumed to follow power laws within the range of 15 to 65 MHz, with exponents α' and α'', such that $G(f) = G_0(f/f_0)^{\alpha}$. The film density was assumed to be 1.0 g/cm^3. The fitting procedure is described in detail in previous studies.[69]

Contact angle measurements. Contact angles were measured using an OCA 35 instrument (DataPhysics Instruments GmbH, Germany). Measurements were performed on the gold sensors in contact with 5 μL drops of ultrapure water. Contact angle values (θ) were calculated as mean ± SE from at least 3 measurements, with drops being positioned on different places on the surface. For the binary SAMs, the fractions of their components were estimated using the Cassie's law:[70]

$$\cos\theta = f_1 \cos\theta_1 + f_2 \cos\theta_2 \quad (2)$$

where θ, θ_1, θ_2 are the contact angles on the mixed SAM and the two pure SAMs, respectively, and f_1 and f_2 are the fractions of each component present in the mixed SAM.

Atomic force microscopy (AFM). The roughness of the gold surface was studied by AFM. Topography images of gold-coated quartz crystals were obtained with a Bruker Dimension Icon microscope in peak force tapping mode using

aluminum-coated silicon nitride cantilevers having a spring constant of 0.4 N/m and a resonance frequency of 70 kHz. AFM images (SI, Fig. S1) were recorded in air and analyzed using Gwyddion software. The obtained root mean square (rms) roughness was 1.1 ± 0.1 nm (average ± SE from 3 independent measurements).

3. RESULTS AND DISCUSSION

Several parameters were tuned to study the influence of surface chemistry on the electrochemical behavior of Fc SAMs and their complexation with β-CD. Table S1 summarizes thiolated molecules and SAM compositions used in this work to study the role of Fc grafting method (direct self-assembly *versus* post-functionalization), Fc linker (alkyl, EG, mixed alkyl/EG), Fc surface density (Γ_{Fc}) and the diluting thiol used to tune Γ_{Fc} (alkyl versus mixed alkyl/EG). The studied Fc SAMs, β-CD derivatives and tunable parameters are illustrated in Fig. 1.

Redox properties of SAMs were characterized by cyclic voltammetry (Figs. 2-4). E-QCM-D measurements were performed on selected samples to characterize the efficiency and redox sensitivity of host/guest interactions between Fc SAMs and soluble β-CD (Fig. 5) and HA-β-CD (Figs. 5-7). Additional QCM-D experiments were performed to characterize the repellent properties of SAMs (Fig. 4C, Fig. S2) and to confirm the specificity of host/guest complexation (Fig. 5B and E). Hydrophilic/hydrophobic properties of Fc SAMs were characterized by contact angle goniometry. The representative images and mean values of contact angles are provided in Figs. 2-4. Below we discuss the obtained results with a focus on the influence of studied parameters on the physico-chemical properties of Fc SAMs and on the resulting host/guest interactions between Fc SAMs and soluble β-CD derivatives.

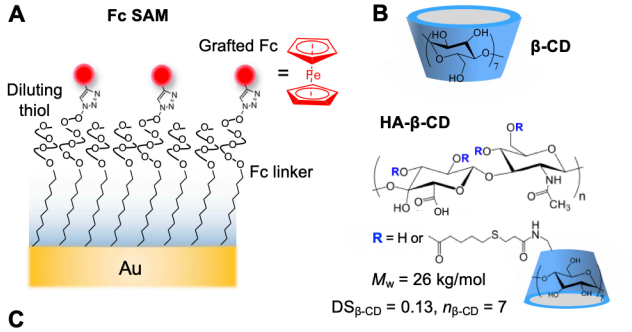

Fig. 1. Tunable β-CD/Fc system to study the role of surface chemistry in host/guest interactions. (A) Schematic of Fc SAMs formed on Au surfaces. An example corresponding to SAM^{click} $Fc^{C11/EG}$-$OH^{C11/EG}$ is shown. Fc chemical structure is shown in red. **(B)** Chemical structures of β-CD and HA-β-CD synthesized by thiol–ene coupling between HA-pentenoate and β-CD-thiol.[16] An average number of β-CD per HA, $n_{β-CD}$ = 7, was calculated based on the initial M_w of HA (20 kg/mol) and $DS_{β-CD}$=0.13 determined by ^{1}H NMR. **(C)** List of tunable parameters.

3.1. Effect of surface chemistry on Fc SAM properties

We coupled cyclic voltammetry, QCM-D and contact angle measurements to study the effect of surface chemistry on the organization, surface density and repellant properties of Fc SAMs. Three interfacial parameters were tuned systematically (i.e., one parameter at a time): i) Fc grafting method, ii) nature of the Fc linker and iii) nature of the diluting thiol (Fig. 1).

3.1.1. Fc grafting method. Direct self-assembly on surfaces and post-functionalization of pre-formed monolayers are the most common methods to form guest SAMs. Previous studies on directly formed Fc SAMs revealed the presence of several Fc populations, including isolated and clustered guest moieties.[40,41,61–63] Such behavior was reported not only on polycrystalline but also on single crystal metal surfaces,[61] highlighting that surface roughness is not the only parameter which governs this heterogeneity. It was suggested that the interchain interactions of Fc alkanethiols in solution and on surfaces both contribute to their 2D clustering.[41,62] Different strategies have been tested to improve SAM homogeneity, including dilution of guest fraction in solution,[40,41,61] replacement of water by organic solvents[63] and addition of physisorbed diluents.[62] Post-functionalization of SAMs could be a more versatile approach, avoiding such adjustments. Although the formation of heterogeneous SAMs was not reported in the case of post-functionalization,[16,35,37,38] a direct comparison between the two methods is needed to assess their benefits and drawbacks under the same conditions.

Using cyclic voltammetry and contact angle goniometry, we compared surface density, homogeneity and hydrophobic properties of Fc SAMs formed on polycrystalline gold surfaces (rms roughness = 1.1 ± 0.1, Fig. S1) by direct self-assembly and by SAM post-functionalization. Same Fc linkers and diluting thiols were used in both approaches so that the only difference between the two systems is the additional step of Fc grafting by click chemistry (Fig. 2A). In the case of direct grafting (Fig. 2A left), Fc SAMs were formed by self-assembly of HS-$(CH_2)_{11}$-Fc or its mixture with the diluting thiol HS-$(CH_2)_{10}$-CH_3 on gold surfaces, resulting in SAM Fc^{C11} or SAM Fc^{C11}-CH_3^{C10}, respectively. In the case of post-functionalization (Fig. 2A right), Fc SAMs were formed in two steps. First, azide-displaying SAMs were obtained by self-assembly of HS-$(CH_2)_{11}$-N_3 or its mixture with HS-$(CH_2)_{10}$-CH_3 on gold surfaces, followed by Cu(I)-catalyzed click reaction with Fc-alkyne, resulting in SAM^{click} Fc^{C11} or SAM^{click} Fc^{C11}-CH_3^{C10}, respectively.

The efficiency of the Fc SAMs formation *via* the two approaches was monitored by contact angle goniometry. The representative images of a water drop deposited on the surfaces functionalized using the two methods are shown in Figs. 2A. The data correspond to the diluted SAM Fc^{C11}-CH_3^{C10} and SAM^{click} Fc^{C11}-CH_3^{C10} formed using 20% of functional thiols in solutions. The data for 100% Fc SAMs is shown in Fig. S3A. The calculated contact angles are listed in Fig. 2C. Regarding the mono-component monolayers, SAM CH_3^{C10} exhibits more hydrophobic properties as compared to SAM N_3^{C11} and SAM Fc^{C11}. Contact angles obtained for HS-$(CH_2)_{11}$-N_3/HS-$(CH_2)_{10}$-CH_3 SAMs are in agreement with those reported for similar systems such as HS-$(CH_2)_{11}$-N_3/HS-$(CH_2)_9$-CH_3 and HS-$(CH_2)_{12}$-N_3/HS-$(CH_2)_9$-CH_3.[36,38] As

expected, the contact angles of the mixed SAMs lie between those of single-component SAMs, confirming that both methods allow tuning Fc surface density (Fig. 2C).

The organization and surface density of Fc moieties in the Fc SAMs obtained by the two methods were characterized by cyclic voltammetry. Fig. 2B shows characteristic CVs obtained for the 20%-diluted SAM Fc^{C11}-CH_3^{C10} and SAM^{click} Fc^{C11}-CH_3^{C10}. The data obtained for the 100% SAM Fc^{C11} and SAM^{click} Fc^{C11} are shown in Fig. S3B. The shape of the redox response obtained for the directly formed Fc SAMs (red curves in Figs. 2B, S3B) indicate the presence of several distinct Fc populations, in agreement with previous studies.[40,41,61,62] In contrast, only one redox peak is observed in the case of post-functionalized Fc SAMs (blue curves in Figs. 2B, S3B). Considering that the two grafting methods are compared under the same conditions (same Fc linker, same diluting thiol, same solvent), one can conclude that homogeneity of guest SAMs can be drastically improved by extending surface functionalization protocol from one-step self-assembly to two-step grafting *via* SAM post-functionalization.

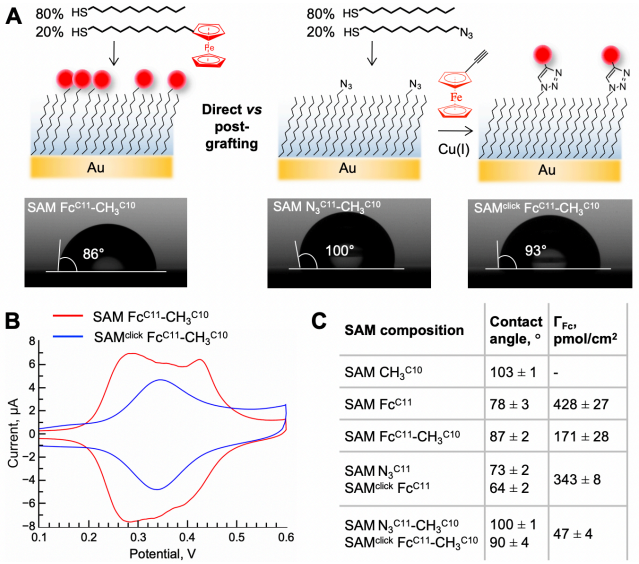

SAM composition	Contact angle, °	Γ_{Fc}, pmol/cm²
SAM CH_3^{C10}	103 ± 1	-
SAM Fc^{C11}	78 ± 3	428 ± 27
SAM Fc^{C11}-CH_3^{C10}	87 ± 2	171 ± 28
SAM N_3^{C11} SAM^{click} Fc^{C11}	73 ± 2 64 ± 2	343 ± 8
SAM N_3^{C11}-CH_3^{C10} SAM^{click} Fc^{C11}-CH_3^{C10}	100 ± 1 90 ± 4	47 ± 4

Fig. 2. Dependence of Fc SAM properties on Fc grafting method. (A) Schematic of SAM Fc^{C11}-CH_3^{C10} and SAM^{click} Fc^{C11}-CH_3^{C10} formed on Au through direct self-assembly or post-functionalization, with characteristic contact angle images. Chemical structures of thiols and Fc-alkyne are shown on top. **(B)** Representative CVs obtained for the diluted Fc SAMs (0.1 M KPF_6, scan rate: 0.1 V/s). **(C)** Contact angles and Γ_{Fc} determined for different SAM compositions; mean ± SE are calculated by averaging results from different samples (n=2-5).

Fig. 2C lists Γ_{Fc} values derived from the integration of the Fc/Fc^+ oxidation peaks (eq. 1). Regarding the directly formed SAMs, Γ_{Fc} obtained for 100% SAM Fc^{C11} gives the average Fc surface area of 38.8 Å², which is in good agreement with the reported footprint for HS-$(CH_2)_{11}$-Fc self-assembled on polycrystalline gold surface.[62] By modelling Fc groups as spheres of 0.66 nm diameter, a surface coverage of 450 pmol/cm² is calculated,[71] leading to a theoretical Fc footprint area of 36.9 Å². This slightly smaller value compared to the measured one can be linked to the poor organization of SAM Fc^{C11}, reflected in different orientations of alkyl chains, as has been suggested previously.[62] As expected, lower Γ_{Fc} was obtained for the 20%-diluted SAM Fc^{C11}-CH_3^{C10}, corresponding to 40 % of the Fc coverage obtained for SAM Fc^{C11} (Fig. 2C). Assuming HS-$(CH_2)_{10}$-CH_3 footprint equal to 21.4 Å²,[71] and HS-$(CH_2)_{11}$-Fc footprint equal to 38.8 Å² (in the case of clusters) or 21.4 Å² (in the case of isolated moieties), one can estimate the HS-$(CH_2)_{11}$-Fc fraction on the surface as 22-27 %, which is close to that in solution (20%). On the other hand, higher fractions of Fc-terminated thiols on the surface as compared to that in solution were reported for other alkylthiolate binary Fc SAMs such as HS-$(CH_2)_{12}$-Fc/HS-$(CH_2)_9$-CH_3 and HS-$(CH_2)_{16}$-Fc/HS-$(CH_2)_{10}$-OH.[40,41] This discrepancy can be attributed to the equal length of the two alkyl chains in our system, in contrast to the longer Fc thiols in the reported studies, a parameter that is likely to be important in adjusting the surface density of Fc in the directly generated Fc SAMs.

Regarding post-functionalized SAMs and assuming the maximal theoretical surface density of HS-$(CH_2)_{11}$-N_3 equal to 776 pmol/cm², which corresponds to the footprint of alkyl thiol of 21.4 Å² [71], only 44% of the total azide population appears to be functionalized with Fc in the case of SAM^{click} Fc^{C11} (Fig. 2C). This result is in the range with previously reported click efficiencies, which did not exceed 50-60% for Fc SAMs based on azide-terminated alkyl thiols.[38] A much lower Γ_{Fc} value is obtained for the diluted SAM^{click} Fc^{C11}-CH_3^{C10}, confirming that Fc surface density can be efficiently tuned by varying thiols ratio in solution (Fig. 2C). Quantitatively, reducing HS-$(CH_2)_{11}$-N_3 fraction in solution to 20%, yielded 14% of the Fc coverage obtained for the saturated SAM^{click} Fc^{C11}. Given quite close contact angle values obtained for pure and mixed SAMs, the estimated surface fraction of HS-$(CH_2)_{11}$-N_3 lies in the range of 3-17 % (eq. 2). Assuming the total coverage equal to 776 pmol/cm²,[71] and given the obtained Γ_{Fc} (Fig. 2C), the minimal click conversion efficiency should be equal to 35%.

Overall, while allowing better organization of Fc SAMs, post-functionalization results in lower Fc surface densities as compared to the direct grafting, being limited to 76 % of the maximal theoretical Fc coverage. This has been related to the steric bulk of the ferrocenes that prevent further conversion of azides to triazoles.[38] As we show in the next section, this limitation depends on the nature of the Fc linker and can be overcome by increasing its flexibility at the solution-facing end.

3.1.2. Fc linker. In the next set of experiments, we fixed the Fc grafting method to the SAM post-functionalization through azide/alkyne click reaction (Fig. 2A right) and varied the nature of Fc linker. We compared three azide-terminated linkers: -$(CH_2)_{11}$- alkyl chain (C11-N_3), -$(CH_2$-CH_2-$O)_{12}$- ethylene glycol chain (EG-N_3) and mixed -$(CH_2)_{11}$-$(CH_2$-CH_2-$O)_6$- chain (C11/EG-N_3) (Fig. 3A). We chose alkyl and ethylene glycol derivatives, because they are widely used in SAM preparation, including guest monolayers.[17,18,38,40–42,60–62] The three linkers were studied under the same conditions (same surface chemistry, same Fc derivative, same solvent) to understand the effect of the linker nature, and in particular its hydrophobicity and flexibility, on the organization and properties of Fc SAMs.

Self-assembly of the C11-N_3, EG-N_3 and C11/EG-N_3 linkers on the gold surface and their click functionalization resulted in SAM^{click} Fc^{C11}, SAM^{click} Fc^{EG} and SAM^{click} Fc$^{C11/EG}$, respectively. The formation of N_3 SAMs, their click functionalization and the resulting changes in their hydrophilic/hydrophobic characteristics were monitored by contact angle measurements. Fig. 3A shows the schematics of the obtained Fc SAMs together with characteristic contact angle images. The determined contact angles are summarized in Fig. 3C. The hydrophobicity of azide-terminated monolayers increased in the order SAM^{click} N_3^{EG} < SAM^{click} $N_3^{C11/EG}$ < SAM^{click} N_3^{C11}, in accordance with the nature of N_3 linkers. All three SAMs showed significant changes in wetting properties after their click functionalization, indicating successful grafting of Fc. More specifically, conjugation with Fc increased hydrophobicity of EG-terminated SAMs (SAM^{click} Fc^{EG} and SAM^{click} Fc$^{C11/EG}$), while opposite effect was observed for alkyl monolayers (SAM^{click} Fc^{C11}). The latter could be explained by the contribution of the triazole groups in the resulting hydrophilic/hydrophobic balance. The trends observed on single-component SAMs (Fig. 3) were reproduced on mixed monolayers (SAM^{click} Fc^{C11}-CH_3^{C10} in Fig. 2 and SAM^{click} Fc$^{C11/EG}$-$OH^{C11/EG}$ in Fig. 4).

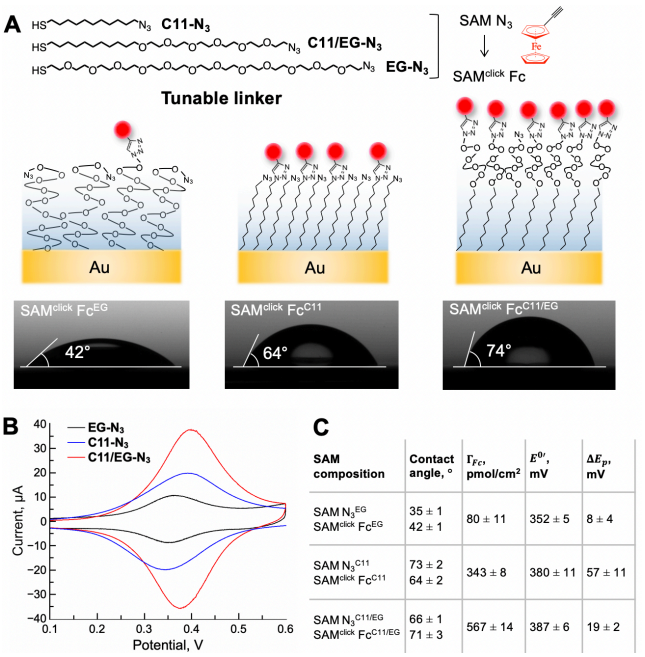

SAM composition	Contact angle, °	Γ_{Fc}, pmol/cm^2	$E^{0\prime}$, mV	ΔE_p, mV
SAM N_3^{EG} / SAM^{click} Fc^{EG}	35 ± 1 / 42 ± 1	80 ± 11	352 ± 5	8 ± 4
SAM N_3^{C11} / SAM^{click} Fc^{C11}	73 ± 2 / 64 ± 2	343 ± 8	380 ± 11	57 ± 11
SAM $N_3^{C11/EG}$ / SAM^{click} $Fc^{C11/EG}$	66 ± 1 / 71 ± 3	567 ± 14	387 ± 6	19 ± 2

Fig. 3. Dependence of Fc SAM properties on the nature of Fc linker. (A) Schematic of SAM^{click} Fc^{EG}, SAM^{click} Fc^{C11} and SAM^{click} Fc$^{C11/EG}$ formed on Au surfaces through post-functionalization of azide-terminated SAMs, with characteristic contact angle images. Chemical structures of different linkers are shown on top. **(B)** Representative CVs obtained for Fc SAMs with different linkers (0.1 M KPF_6, scan rate: 0.1 V/s). **(C)** Determined contact angles, Γ_{Fc}, ΔE_p and $E^{0\prime}$; mean ± SE are calculated by averaging results obtained on different samples (n=2-4).

The effect of Fc linker on the organization and redox properties of Fc SAMs was characterized by cyclic voltammetry (Fig. 3B). In addition to the Fc surface density Γ_{Fc}, the formal potential $E^{0\prime}$ and anodic/cathodic peak difference ΔE_p have been determined from the recorded CVs (Fig. 3C). Fig. 3B shows the examples of CVs recorded for SAM^{click} Fc^{EG} (black), SAM^{click} Fc^{C11} (blue) and SAM^{click} Fc$^{C11/EG}$ (red). All systems show one oxidation and one reduction peak, indicating the absence of clustered Fc domains in post-functionalized SAMs, regardless of the Fc linker. Fitting the oxidation peaks to a Gaussian distribution[40] showed that all systems exhibit symmetric responses with larger peak widths compared to the ideal electrochemical response of diluted Fc SAMs (about 90 mV[71]), with the stronger deviation being obtained in the case of SAM^{click} Fc^{C11} (Fig. S4). The latter can be attributed to the rigidity of the alkyl SAMs, which, together with the non-complete azide conversion, may result in the presence of populations with different local densities of Fc. The larger distribution of distances between Fc moieties could result the larger differences in the electron transfer process, which has been shown to involve hopping,[39,60,66] leading to broader redox peaks comprising numerous populations with slightly different peak positions.

One can note a strong relation between the nature of the Fc linker and the resulting Fc surface density. Indeed, when EG-N_3 is replaced by C11-N_3, Γ_{Fc} increases from 18 to 76 % of the theoretical Fc coverage (450 pmol/cm^2 [71]), while values even exceeding this theoretical maximum (128 %) are obtained in the case of the C11/EG-N_3 linker. Similar trend was detected for the hydrophobicity of Fc SAMs (Fig. 3A, C), in agreement with the obtained differences in Γ_{Fc}. In contrast to C11 chains, which are known to form densely packed SAMs, hydrophilic and flexible EG chains are expected to form more diluted monolayers. Indeed, the reported densities of ferrocene in directly formed Fc SAMs composed of EG chains are in the range from 200 to 300 pmol/cm^2,[60] which is considerably lower than that obtained for the directly formed SAMs composed of alkyl chains studied here (~ 430 pmol/cm^2, Fig. 2B, C) and by other groups.[40,62] The surface density of azide groups is thus expected to be higher in the case of the C11-N_3 and C11/EG-N_3 linkers as compared to the EG-N_3 linker. To confirm this reasoning, we have determined the density of the azide SAMs by SPR, which yielded Γ_{N3} = 382 ± 24, 650 ± 41 and 829 ± 52 pmol/cm^2 for SAM N_3^{EG}, SAM $N_3^{C11/EG}$ and SAM N_3^{C11}, respectively (Table S2, see SI for the details of SPR experiments). The value obtained for SAM N_3^{C11} is close to what is predicted theoretically for alkyl SAMs (776 pmol/cm^2); slightly higher packing could be related to the roughness of gold coatings (Fig. S1). Somewhat lower coverage was obtained for SAM $N_3^{C11/EG}$, which can be related to the presence of OEG-N_3 extremities. Given the Γ_{N3} values determined by SPR and Γ_{Fc} values determined electrochemically, the conversion efficiency of azide in triazole can be calculated as 21, 87 and 41 % for SAM N_3^{EG}, SAM $N_3^{C11/EG}$ and SAM N_3^{C11}, respectively.

Because of the formation of dense SAMs, as confirmed by the obtained Γ_{N3} (Table S2), both C11-N_3 and C11/EG-N_3 linkers should be extended towards the solution, making the azide groups available for the click reaction. In contrast, some azide groups may be hidden inside the more diluted monolayer composed of EG-N_3, as EG chains are assumed to be less stretched than C11 and C11/EG. Therefore, the lowest Γ_{Fc} obtained for SAM^{click} Fc^{EG} (Fig. 3B, C) may be due to both the low density and poor availability of azide groups in this system. Furthermore, the higher Γ_{Fc} obtained for SAM^{click} Fc$^{C11/EG}$ as compared to SAM^{click} Fc^{C11} (Fig. 3B, C),

despite the lower Γ_{N3} obtained for C11/EG (Table S2), can be related to the greater flexibility of the EG terminus, which allows the C11/EG-N_3 linker to overcome steric barriers more easily and accommodate more Fc moieties in the monolayer as compared to the rigid C11-N_3 linker.

Regarding other electrochemical parameters, higher $E^{0'}$ values were obtained for SAM^{click} Fc^{C11} and SAM^{click} Fc$^{C11/EG}$ as compared to SAM^{click} Fc^{EG} (Fig. 3B, C). This difference could be related to the less polar environment (due to the presence of C11 chains), which requires a higher polarization energy, leading to the positive shift of the formal potential.[41,62] This is consistent with the much higher hydrophilic properties of SAM^{click} Fc^{EG} as compared to SAM^{click} Fc^{C11} and SAM^{click} Fc$^{C11/EG}$ (Fig. 3A, C). In addition, the presence of neighboring ferrocenium cations impedes the removal of electrons from the remaining Fc during oxidation, which should be more pronounced in SAMs with higher Γ_{Fc}.[40,41,63] The latter explanation is in line with the increase of $E^{0'}$ with Γ_{Fc} at fixed SAM composition: 342 ± 8 and 380 ± 11 mV are obtained for 20% SAM^{click} Fc^{C11}-CH_3^{C10} (Γ_{Fc} = 47 ± 4 pmol/cm², Fig. 2B, C) and 100% SAM^{click} Fc^{C11} (Γ_{Fc} = 343 ± 8 pmol/cm², Fig. 3B, C), respectively. Besides, an increase in ΔE_p is observed in the order SAM^{click} Fc^{EG} < SAM^{click} Fc$^{C11/EG}$ < SAM^{click} Fc^{C11}. Previous studies pointed out the importance of Fc interactions with hydrophobic anions (here PF_6^-), which were shown to form organized monolayers at high Fc densities, slowing down the electron transfer kinetics.[64] This effect should be more pronounced on alkyl SAMs due to their hydrophobic nature and rigidity, which may explain the drastic increase of ΔE_p in the case of SAM^{click} Fc^{C11}. This interpretation is supported by considerably lower ΔE_p value obtained for the diluted SAM^{click} Fc^{C11}-CH_3^{C10} (9 ± 2 mV, example is shown in Fig. 2B, blue).

Taken together, our results show that mixed linkers like C11/EG-N_3 are preferable for the formation of Fc SAMs as they provide both homogeneous distribution of Fc moieties and high Fc surface density. In our previous studies, we showed that guest surface density can be varied in a wide range by mixing C11/EG-N_3 with diluting thiols of similar nature.[16,17] Below we describe our study of the effect of the type of the diluting thiol on the interfacial properties of Fc SAMs.

3.1.3. Diluting thiol. For the next series of experiments, we fixed Fc linker to C11/EG-N_3 and prepared diluted Fc SAMs through the post-functionalization approach (Fig. 2A, right), while tuning the nature of the diluting thiol. Two diluting thiols were compared: -$(CH_2)_{11}$- alkyl chain (C11) and mixed -$(CH_2)_{11}$-$(CH_2$-CH_2-$O)_4$- chain (C11/EG) (Fig. 4A). SAM^{click} Fc$^{C11/EG}$-CH_3^{C10} and SAM^{click} Fc$^{C11/EG}$-$OH^{C11/EG}$ were obtained by co-immobilization of C11/EG-N_3 (20%) with C11 or C11/EG (80%), followed by Fc grafting by azide/alkyne click reaction (Fig. 4A). The successful formation of N_3 SAMs and their click-functionalization were confirmed by contact angle measurements, which also allowed to estimate the fraction of azide thiols on the surface (eq. 2). Representative water drop images and the determined contact angles before and after click reaction are shown in Fig. 4A and D.

The contact angle values obtained for the diluted SAM $N_3^{C11/EG}$-CH_3^{C10} and SAM $N_3^{C11/EG}$-$OH^{C11/EG}$ (Fig. 4D) lie between that of pure SAM $N_3^{C11/EG}$ and SAM CH_3^{C10} or SAM $OH^{C11/EG}$, respectively (Fig. 4E). One can note the good agreement between the obtained contact angles and previously reported values for the pure SAM $N_3^{C11/EG}$, SAM $OH^{C11/EG}$, SAM CH_3^{C10} and mixed SAM $N_3^{C11/EG}$-$OH^{C11/EG}$.[35,36] Compared to SAM $N_3^{C11/EG}$-$OH^{C11/EG}$, the wetting properties of SAM $N_3^{C11/EG}$-CH_3^{C10} are closer to those of pure SAM $N_3^{C11/EG}$ (Fig. 4D). Quantitatively, applying Cassie's law (eq. 2) to the two cases yields 69 and 14% of C11/EG-N_3 in SAM $N_3^{C11/EG}$-CH_3^{C10} and SAM $N_3^{C11/EG}$-$OH^{C11/EG}$, respectively. Higher fraction of C11/EG-N_3 in SAM $N_3^{C11/EG}$-CH_3^{C10} can be explained by the preferential adsorption of the longer C11/EG-N_3 linker when mixed with the shorter C11 diluting thiol.

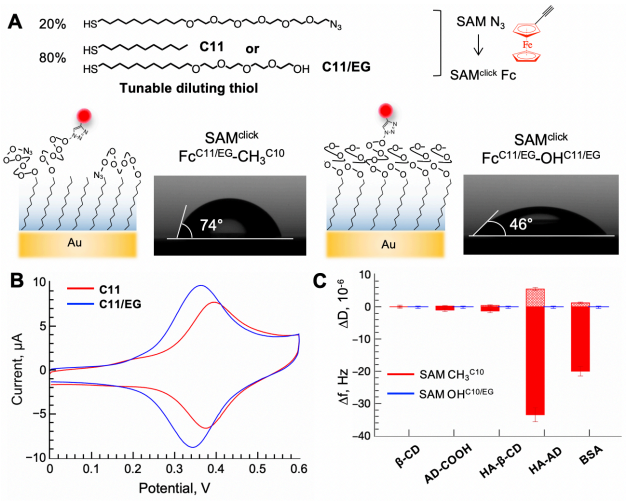

D

Diluted SAMs	Contact angle, °	Γ_{Fc}, pmol/cm²	$E^{0'}$, mV	ΔE_p, mV
SAM $N_3^{C11/EG}$-CH_3^{C10}	78 ± 3	71 ± 11	379 ± 2	13 ± 2
SAM^{click} Fc$^{C11/EG}$-CH_3^{C10}	74 ± 1			
SAM $N_3^{C11/EG}$-$OH^{C11/EG}$	39 ± 1	108 ± 5	356 ± 2	22 ± 1
SAM^{click} Fc$^{C11/EG}$-$OH^{C11/EG}$	46 ± 1			

E

Pure SAMs	Contact angle, °
SAM $N_3^{C11/EG}$	66 ± 1
SAM CH_3^{C10}	103 ± 2
SAM $OH^{C11/EG}$	33 ± 1

Fig. 4. Dependence of Fc SAM properties on the nature of the diluting thiol. (A) Schematic of SAM^{click} Fc$^{C11/EG}$-CH_3^{C10} and SAM^{click} Fc$^{C11/EG}$-$OH^{C11/EG}$ formed on Au surfaces through post-functionalization of azide-terminated diluted SAMs, with characteristic contact angle images. Chemical structures of thiolated derivatives are shown on top. **(B)** Representative CVs registered for Fc SAMs obtained using different diluting thiols (0.1 M KPF_6, scan rate: 0.1 V/s). **(C)** QCM-D response (negative Δf and positive ΔD) recorded for the binding of β-CD, AD-COOH, HA-β-CD and HA-AD (HA functionalized with AD, see Fig. S2 for details) to SAM CH_3^{C10} (red) and SAM $OH^{C11/EG}$ (blue). Examples of raw QCM-D data and experimental conditions are given in Fig. S2. **(D)** Contact angles, Γ_{Fc}, $E^{0'}$ and ΔE_p determined for the diluted SAMs. **(E)** Contact angles determined for the mono-component SAMs. Mean ± SE shown in (D-E) are calculated by averaging results obtained on different samples (n=2-4).

Cyclic voltammetry was used to characterize the organization of Fc SAMs and to quantify their redox characteristics, while tuning the nature of the diluting thiol (Fig. 4B, D). Fig. 4B shows the examples of CVs obtained for SAM^{click} Fc$^{C11/EG}$-CH_3^{C10} (red) and SAM^{click} Fc$^{C11/EG}$-$OH^{C11/EG}$ (blue). A single redox peak was detected in both cases, indicating a homogeneous distribution of Fc moieties, irrespective of the diluting thiol. Γ_{Fc}, $E^{0'}$ and ΔE_p, determined from voltammograms, are listed in Fig. 4D. Assuming the maximal

coverage of the surface by C11/EG chains equal to 776 pmol/cm² (at the theoretical footprint of alkyl chains of 21.4 Å²),[71] the Γ_{Fc} value obtained for SAM^{click} Fc$^{C11/EG}$-OH$^{C11/EG}$ corresponds to 14 % of functionalized C11/EG chains. Given the contact angles obtained for the mixed SAM^{click} Fc$^{C11/EG}$-OH$^{C11/EG}$ and pure SAM $N_3^{C11/EG}$ and SAM OH$^{C11/EG}$ (Fig. 4D, E), the estimated fraction of C11/EG-N_3 in SAM^{click} Fc$^{C11/EG}$-OH$^{C11/EG}$ is 14% (eq. 2). The perfect match between the calculated fraction of C11/EG-N_3 on the surface and the estimated fraction of C11/EG chains functionalized with Fc suggests that the yield of the click reaction approaches 100% in the diluted SAM^{click} Fc$^{C11/EG}$-OH$^{C11/EG}$.

Surprisingly, 1.5-times lower Γ_{Fc} values were obtained for SAM^{click} Fc$^{C11/EG}$-CH_3^{C10} as compared to SAM^{click} Fc$^{C11/EG}$-OH$^{C11/EG}$ (Fig. 4B, D), despite the higher density of azide groups expected in the case of SAM $N_3^{C11/EG}$-CH_3^{C10} based on its wetting properties. We hypothesize that this decrease is due to the lower accessibility of azide groups for click reaction in SAM^{click} $N_3^{C11/EG}$-CH_3^{C10}. Indeed, in the absence of the diluting EG chains, flexible EG-N_3 extremities can twist in SAM^{click} Fc$^{C11/EG}$-CH_3^{C10}, allowing azide groups to hide in the hydrophobic part of the monolayer (Fig. 4A left). In contrast, in the case of SAM^{click} Fc$^{C11/EG}$-OH$^{C11/EG}$, C11/EG-N_3 linkers are blocked between C11/EG diluting thiols, which orient OEG-N_3 extremities towards the click solution (Fig. 4A right). Besides, an increase in $E^{0'}$ and decrease in ΔE_p are observed when replacing C11/EG by C11 diluting thiol (Fig. 4B, D). The positive shift of $E^{0'}$ can be related to a less polar environment due to the higher fraction of C11 versus EG chains in SAM^{click} Fc$^{C11/EG}$-CH_3^{C10} (Fig. 4A),[41,62] which is consisted with higher contact angles obtained for SAM^{click} Fc$^{C11/EG}$-CH_3^{C10} (Fig. 4A, D). The slight difference in ΔE_p could be due to the different organization of the Fc moieties, which are supposed to be more ordered and extended away from the electrode in the case of the C11/EG diluting thiol (Fig. 4A).

Given that the formation of host/guest SAMs is often followed by host/guest assembly, suppression of unwanted non-specific interactions is one of the crucial steps in the formation of stimuli-responsive interfaces and should therefore be considered in the choice of diluting thiol. With this in mind, we tested the non-specific binding of several soluble probes on the SAMs composed of the two diluting thiols, i.e. SAM CH_3^{C10} and SAM OH$^{C11/EG}$. Given the well-known repelling properties of EG coatings and strong hydrophobic properties of C11 thiol (Fig. 4E), one would expect stronger non-specific binding to SAM CH_3^{C10}. Fig. 4C shows the results of QCM-D monitoring of binding of monovalent (β-CD, AD-COOH) and multivalent (HA-β-CD, HA-AD) host/guest derivatives as well as protein BSA on SAM CH_3^{C10} and SAM OH$^{C11/EG}$. The presented shifts in frequency (Δf) reflect the mass uptake on the QCM-D sensors functionalized with SAM CH_3^{C10} or SAM OH$^{C11/EG}$ upon their exposure to the soluble probes (see Fig. S2 for QCM-D profiles). Remarkably, no binding was detected on SAM OH$^{C11/EG}$, while almost all probes showed binding to SAM CH_3^{C10}, in particular HA-AD representing hydrophilic polymer (hyaluronic acid) bearing hydrophobic units (AD) and BSA. The latter could be explained by hydrophobic interactions between these two probes and SAM CH_3^{C10}. These different repellent properties should be considered when constructing host/guest assemblies on surfaces, especially on strongly diluted SAMs.

3.2. Effect of surface chemistry on β-CD/Fc binding

The effect of surface chemistry on host/guest interactions was studied using QCM-D *in situ* coupled to electrochemistry (E-QCM-D). Fc SAMs were exposed to two soluble host probes: monovalent β-CD and multivalent HA-β-CD (Fig. 1B). Incubation with β-CD probes and subsequent rinsing were done in a flow mode at 20 µL/min. Several parameters were compared while tuning interfacial properties of Fc SAMs, including the efficiency of β-CD/Fc binding and its reversibility under redox stimuli. Viscoelastic modeling of QCM-D data was used to determine the amount of attached β-CD probe and to estimate the efficiency of its detachment upon Fc oxidation.

3.2.1. Monovalent β-CD *versus* multivalent HA-β-CD. The choice of β-CD and HA-β-CD was motivated by the simplicity of monovalent complexation on one side and a wide use of various multivalent scaffolds in material and life sciences on another side. In order to compare the suitability of these two probes for our study, Fc SAM composition was fixed to SAM^{click} Fc$^{C11/EG}$-OH$^{C11/EG}$, which was expected to suppress undesired non-specific interactions (Fig. 4C), and its interactions with β-CD (Fig. 5A) and HA-β-CD (Fig. 5D) were monitored by E-QCM-D. The fraction of HS-$(CH_2)_{11}$-N_3 in solution was fixed to 10-20 % resulting in Γ_{Fc} = 55 - 115 pmol/cm². SAM OH$^{C11/EG}$ was used as a control surface lacking guest moieties. Based on the affinity of β-CD/Fc complexation (reported K_d values in solution vary from 0.2 to 0.7 mM),[72–75] β-CD concentration was fixed to 5 mM. Assuming much higher binding strength due to the multivalency of HA-β-CD ($n_{β\text{-}CD}$ = 7, Fig. 1B) and based on the binding assays described,[16,17] HA-β-CD concentration was fixed to 50 µg/mL, which corresponds to 1.9 µM of HA-β-CD chains and 12 µM of β-CD moieties displayed by HA-β-CD chains (based on $DS_{β\text{-}CD}$ = 13%). The characteristic QCM-D profiles together with the CVs recorded in parallel are shown in Figs. 5B, C for β-CD and in Figs. 5E, F for HA-β-CD.

One can note similar frequency (Δf) and dissipation (ΔD) shifts upon injection of 5 mM β-CD to SAM^{click} Fc$^{C11/EG}$-OH$^{C11/EG}$ (Fig. 5B, solid lines) and to the control surface SAM OH$^{C11/EG}$ (Fig. 5B, dashed lines). The fact that no response was detected on SAM OH$^{C11/EG}$ at 10-times lower β-CD concentration (Fig. 4C, blue) suggests that the observed shifts on SAM OH$^{C11/EG}$ (Fig. 5B, dashed lines) are most likely due to the increase in density and viscosity of the electrolyte solution in the presence of concentrated 5 mM β-CD. This means that Δf = -3.4 Hz, $\Delta D = 0.9 \cdot 10^{-6}$ obtained for SAM^{click} Fc$^{C11/EG}$-OH$^{C11/EG}$ upon β-CD injection (Fig. 5B, solid lines) are partially induced by changes in the solvent properties and thus are not entirely specific to β-CD binding. In contrast, QCM-D shifts obtained upon injection of diluted HA-β-CD (1.9 µM of HA-β-CD chains *vs* 5 mM β-CD) can be fully attributed to its binding to SAM^{click} Fc$^{C11/EG}$-OH$^{C11/EG}$, since no response was observed on SAM OH$^{C11/EG}$ (Fig. 5E, dashed lines). Higher Δf = - 10.8 Hz and $\Delta D = 1.8 \cdot 10^{-6}$ obtained in the case of HA-β-CD are expected (Fig. 5E, solid lines), given its higher mass compared to β-CD and the ability to form soft hydrated films with loops and tails thanks to the flexibility of polymer chains.

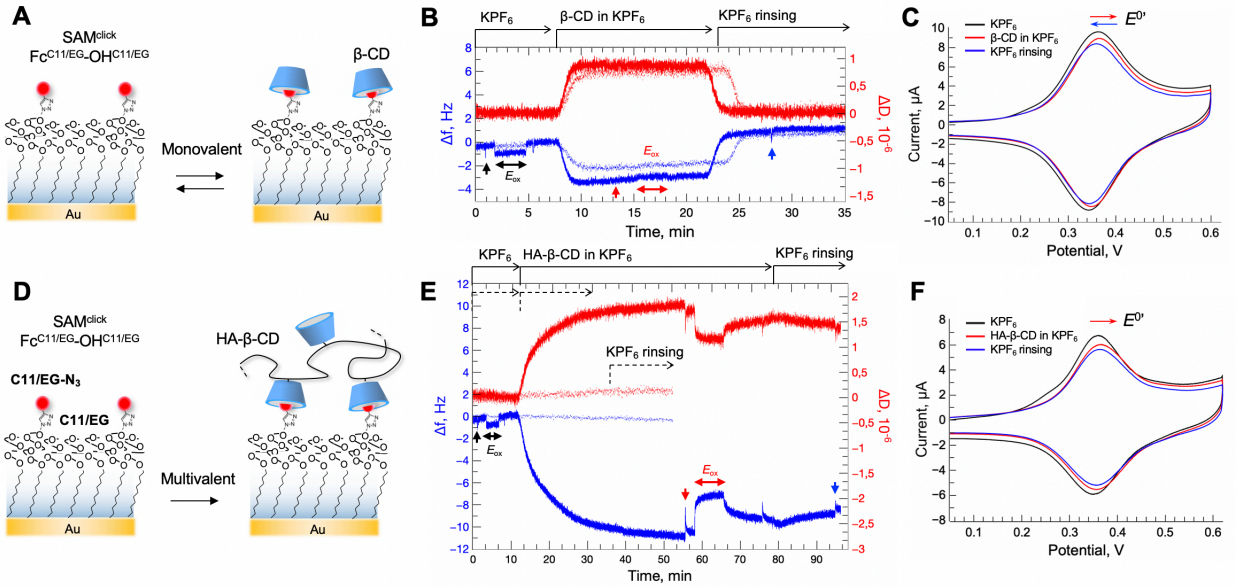

Fig. 5. E-QCM-D monitoring of interactions between Fc SAMs and soluble β-CD probes. (A, D) Schematic of interactions between SAM^{click} Fc$^{C11/EG}$-OH$^{C11/EG}$ and β-CD (A) or HA-β-CD (D). **(B, E)** Representative Δf (blue) and ΔD (red) shifts recorded during exposure of SAM^{click} Fc$^{C11/EG}$-OH$^{C11/EG}$ (solid lines) and SAM OH$^{C11/EG}$ (dashed lines) to β-CD (B) or HA-β-CD (E). The solutions in contact with the surfaces at different moments of time are indicated on the top of QCM-D profiles; solid and dashed arrows in (E) correspond to SAM^{click} Fc$^{C11/EG}$-OH$^{C11/EG}$ and SAM OH$^{C11/EG}$. Vertical arrows of different colors and horizontal black arrows indicate the moments of recording CVs and applying E_{ox}, respectively. **(C, F)** CVs recorded on SAM^{click} Fc$^{C11/EG}$-OH$^{C11/EG}$ in pure electrolyte (black), in the presence of β-CD (C) or HA-β-CD (F) (red) and after rinsing the surface with the electrolyte solution (blue). The moments of recording CVs are indicated by vertical arrows of corresponding colors in QCM-D profiles (B, E). **Conditions**: Γ_{Fc} = 113 pmol/cm^2 (B, C) or 71 pmol/cm^2 (E, F), electrolyte = 0.1 M KPF_6, scan rate = 0.1 V/s, E_{ox} = 0.45 V, $c_{β\text{-}CD}$ = 5 mM, $c_{HA\text{-}β\text{-}CD}$ = 50 μg/mL (1.9 μM of polymer chains), flow rate during β-CD/HA-β-CD injection and rinsing = 20 μL/min (flow stopped during CVs and E_{ox}).

The recorded QCM-D profiles show that, contrary to the reversible binding of β-CD (Fig. 5B), the majority of HA-β-CD remains attached to SAM^{click} Fc$^{C11/EG}$-OH$^{C11/EG}$ upon rinsing (Fig. 5E), as expected in the case of multivalent binding.[16,17] This conclusion agrees with the recorded CVs. Indeed, the small positive shift of redox peaks upon β-CD injection ($\Delta E^{0'}$ = +4 mV) disappeared after rinsing (Fig. 5C), whereas in the case of HA-β-CD, similar shift of $\Delta E^{0'}$ = +7 mV persisted (Fig. 5F). We note that the slight decrease in the current is due to the limited stability of Fc monolayers during relatively long E-QCM-D measurements and is not related to host/guest interactions. The anodic shift of $E^{0'}$ is thus the only electrochemical manifestation of β-CD/Fc binding in our system. The observed positive shift is less pronounced than those reported for β-CD/Fc binding in solution,[32,72] which is probably due to the steric hindrance limiting all Fc to form host/guest complexes on the surface.

The decrease of β-CD/Fc affinity upon Fc oxidation is well known, making β-CD/Fc complexation responsive to electrochemical stimuli, which has been utilized for reversible assemblies of various molecules and nano-objects.[2,5] Application of electrochemical stimuli to SAM^{click} Fc$^{C11/EG}$-OH$^{C11/EG}$ induced characteristic QCM-D shifts, showing similar trends in the case of β-CD and HA-β-CD (Figs. 5B, E). In the absence of host probes, Δf of - 0.8-1.0 Hz was observed upon recording CVs and applying E_{ox} to SAM^{click} Fc$^{C11/EG}$-OH$^{C11/EG}$ (Figs. 5B, E). This fast and reversible response is specific to Fc and, according to previous studies,[76] can be attributed to the flow of PF_6^- anions (together with associated water molecules) towards SAM^{click} Fc$^{C11/EG}$-OH$^{C11/EG}$ upon Fc/Fc$^+$ oxidation. Interestingly, this shift disappeared in the presence of β-CD (Fig. 5B, red arrows) and became positive in the presence of HA-β-CD (Fig. 5E, red arrows), indicating the detachment of host molecules upon Fc oxidation, occurring in parallel with the uptake of PF_6^-. Although the fraction of detached hosts cannot be deduced in the case of β-CD, due to the solvent contribution to the binding response (Fig. 5B), we can clearly conclude that the detachment of HA-β-CD is partial (Fig. 5E). The latter means that the decrease of the affinity of β-CD/Fc$^+$ complexes is not sufficient to brake multivalent bonds between SAM^{click} Fc$^{C11/EG}$-OH$^{C11/EG}$ and HA-β-CD at a given Γ_{Fc} = 71 pmol/cm^2.

The obtained E-QCM-D results prove successful binding of β-CD probes to Fc monolayers (shifts in Δf, ΔD and $E^{0'}$ upon β-CD/HA-β-CD injection, Fig. 5) as well as the sensitivity of β-CD/Fc interactions to electrochemical stimuli (different Δf shifts in the absence/presence of β-CD/HA-β-CD, Fig. 5B, E). Given the specificity of QCM-D response and higher Δf and ΔD shifts obtained in the case of HA-β-CD as well as the stability of HA-β-CD attachment during rinsing, this probe was chosen to study the effect of surface chemistry on β-CD/Fc interactions. Below we describe the obtained results with a focus on the efficiency of β-CD/Fc complexation and its disassembly upon oxidation.

3.2.2. Influence of surface chemistry on HA-β-CD binding to Fc SAMs and its redox-driven detachment. To understand how surface chemistry influences β-CD/Fc complexation, we varied Fc SAM composition and studied its effect on the interaction with HA-β-CD. In the first set of experiments, we formed Fc monolayers by SAM post-

functionalization *via* azide/alkyne click reaction, while varying Fc linker (EG-N_3, C11-N_3, C11/EG-N_3, Fig. 3A) or diluting thiol (C11 *vs* C11/EG, Fig. 4A). The characteristic E-QCM-D profiles are shown in Fig. 6A-C for the tunable Fc linker and in Figs. 5E and 6C for the tunable diluting thiol. Fig. 6D summarizes the hydrated masses of bound HA-β-CD, $\Gamma^{hydrated}_{HA-\beta-CD}$, and fractions of the detached HA-β-CD upon oxidation determined by viscoelastic modeling.

Given that multivalent binding, and in particular β-CD/Fc multivalent interaction, is highly sensitive to the density of surface ligands,[46] we maintained the same surface density of Fc for all investigated Fc SAM compositions (Γ_{Fc}= 50-70 pmol/cm^2, Fig. 6D). This surface density corresponds to the average distance between Fc groups l_{Fc} = 1.5 - 1.8 nm (assuming square lattice). In the case of the EG-N_3 linker, no dilution was done (Fig. 6A) as such surface density was obtained for SAM^{click} Fc^{EG} consisting purely of EG-N_3 linkers (Fig. 3). In the case of C11-N_3 and C11/EG-N_3, 75-90% fraction of C11 (or C11/EG) diluting thiol was used, resulting in SAM^{click} Fc^{C11}-CH_3^{C10} (Fig. 6B) and SAM^{click} Fc$^{C11/EG}$-CH_3^{C10} (Fig. 6C) (or SAM^{click} Fc$^{C11/EG}$-OH$^{C10/EG}$, Fig. 5D, E) with the desired Γ_{Fc}. Other conditions (Fc derivative, solvent, HA-β-CD concentration) were also kept constant to ensure that the observed effects are entirely due to changes in Fc SAM composition.

Remarkably, no interactions with HA-β-CD was detected on SAM^{click} Fc^{EG} composed of flexible EG chains (Fig. 6A), in contrast to all other studied cases (Figs. 5E, 6B and 6C). As discussed above (see Section 3.1.2), the accessibility of azide groups for the click reaction is likely to be reduced by the low packing density and high flexibility of the EG chains. We hypothesize that the same factors account for the poor accessibility of Fc moieties for β-CD complexation, so that the latter are hidden in these flexible coatings as schematically shown in Fig. 6A. The fact that applying oxidation potential to SAM^{click} Fc^{EG} induces not only negative Δf but also positive ΔD (Fig. 6A) might mean that ion/solvent exchange occurs across SAM^{click} Fc^{EG}, matching the picture when Fc groups are located within SAM^{click} Fc^{EG} rather than on its surface.

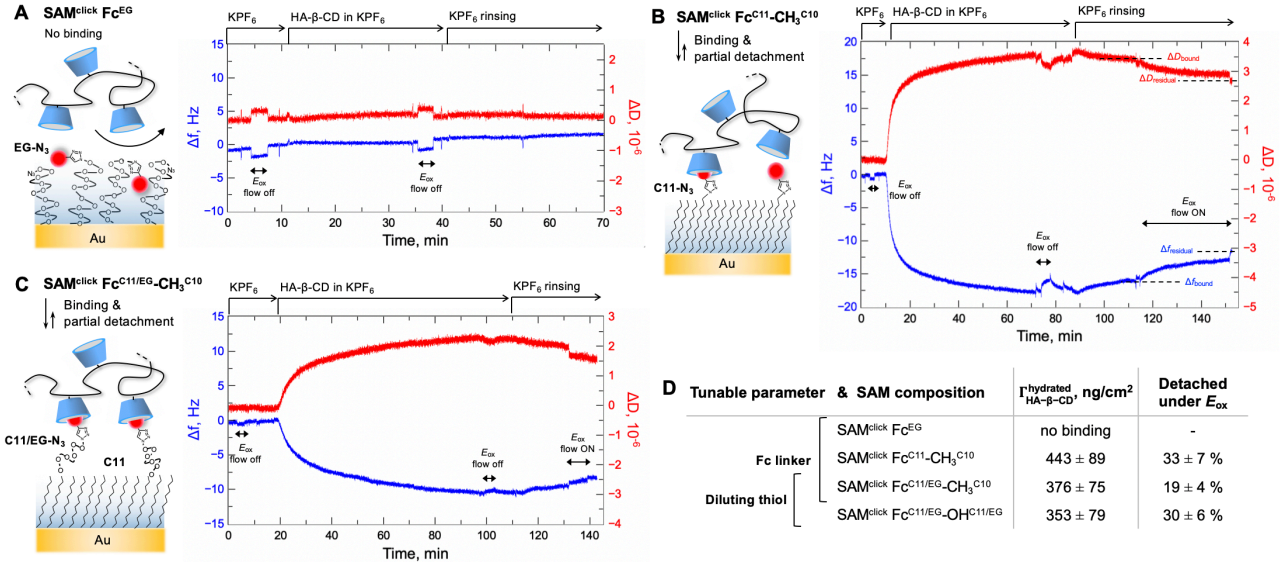

D

Tunable parameter & SAM composition		$\Gamma^{hydrated}_{HA-\beta-CD}$, ng/cm^2	Detached under E_{ox}
Fc linker	SAM^{click} Fc^{EG}	no binding	-
	SAM^{click} Fc^{C11}-CH_3^{C10}	443 ± 89	33 ± 7 %
Diluting thiol	SAM^{click} Fc$^{C11/EG}$-CH_3^{C10}	376 ± 75	19 ± 4 %
	SAM^{click} Fc$^{C11/EG}$-OH$^{C11/EG}$	353 ± 79	30 ± 6 %

Fig. 6. Dependence of β-CD/Fc interactions on the nature of Fc linker and diluting thiol. (A) Schematic showing the absence of interaction between SAM^{click} Fc^{EG} and HA-β-CD concluded based on the absence of QCM-D response during exposure of SAM^{click} Fc^{EG} to HA-β-CD. **(B-C)** Schematic of HA-β-CD binding to SAM^{click} Fc^{C11}-CH_3^{C10} (B) and SAM^{click} Fc$^{C11/EG}$-CH_3^{C10} (C) with representative Δf (blue) and ΔD (red) shifts recorded upon HA-β-CD injection and rinsing accompanied by E_{ox} application; E_{ox} application was stopped once signal is stabilized. **(D)** List of the studied SAM compositions with corresponding masses of hydrated HA-β-CD films, $\Gamma^{hydrated}_{HA-\beta-CD}$, determined by viscoelastic modeling of Δf_{bound} and ΔD_{bound}, and fraction of the detached HA-β-CD, calculated as $(\Gamma^{hydrated}_{HA-\beta-CD}-\Gamma^{residual}_{HA-\beta-CD})/\Gamma^{hydrated}_{HA-\beta-CD}$*100%, where $\Gamma^{residual}_{HA-\beta-CD}$ is determined by viscoelastic modeling of $\Delta f_{residual}$ and $\Delta D_{residual}$; examples of the bound and residual shifts are shown in (B). The case of HA-β-CD binding to SAM^{click} Fc$^{C11/EG}$-OH$^{C11/EG}$, having the same Fc linker but different diluting thiol compared to (C), is shown in Fig. 5E. **Conditions**: Γ_{Fc}= 50-70 pmol/cm^2, electrolyte = 0.1 M KPF_6, E_{ox} = 0.45 V, $c_{HA-\beta-CD}$ = 50 μg/mL (1.9 μM of polymer chains), flow = 20 μL/min. The solutions in contact with the surfaces at different moments of time are indicated on the top of QCM-D profiles. Black arrows indicate the moments of applying E_{ox}.

Comparing HA-β-CD binding to SAM^{click} Fc^{C11}-CH_3^{C10} (Fig. 6B), SAM^{click} Fc$^{C11/EG}$-CH_3^{C10} (Fig. 6C) and SAM^{click} Fc$^{C11/EG}$-OH$^{C10/EG}$ (Fig. 5D), similar QCM-D responses were observed, with a slightly higher response in the case of SAM^{click} Fc^{C11}-CH_3^{C10}. Despite the negligible non-specific interactions between HA-β-CD and Fc SAMs (Fig. 4C), we did not observe complete detachment of HA-β-CD upon Fc oxidation (Fig. 5E, Fig. 6). This suggests that the residual affinity of β-CD/Fc$^+$, accompanied by rather slow kinetics of polymer detachment (Fig. 6), is sufficient to maintain multivalent binding at a given Γ_{Fc} = 50-70 pmol/cm^2. Quantitatively (Fig. 6D), one- third of host probe was detached in the case of SAM^{click} Fc^{C11}-CH_3^{C10} (Fig. 6B). Similar detachment efficiency was observed in the case of SAM^{click} Fc$^{C11/EG}$-OH$^{C10/EG}$ (Fig. 5D), whereas it was 1.7-times lower for SAM^{click} Fc$^{C11/EG}$-CH_3^{C10} (Fig. 6C).

The difference in HA-β-CD binding could be due to different numbers of HA-β-CD molecules attached and/or

different conformations of the HA-β-CD layers. It can be hypothesized that the rigid interfaces consisting of C11 chains may limit the number of β-CD/Fc bonds per HA-β-CD, resulting in HA-β-CD chains being more elongated towards the solution and thus forming more extended and softer coatings, yielding somewhat higher QCM-D response in the case of SAM^{click} Fc^{C11}-CH$_3$^{C10} (Fig. 6B). This explanation is in line with highest detachment efficiency obtained for SAM^{click} Fc^{C11}-CH$_3$^{C10} (Fig. 6B). In contrast, one would expect the highest flexibility of Fc linkers in the case of SAM^{click} Fc$^{C11/EG}$-CH$_3$^{C10} (Fig. 6C), which may contribute to an increase in the number of bonds formed and hence make it more difficult for HA-β-CD to detach.

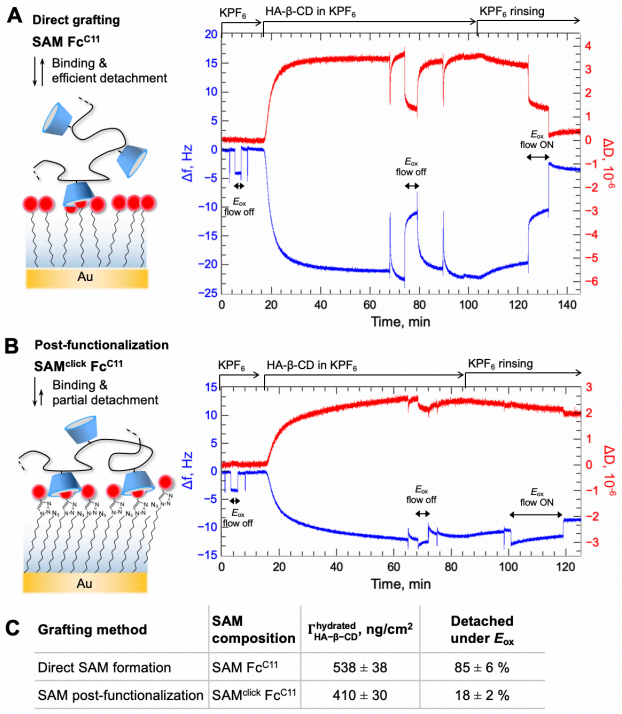

C

Grafting method	SAM composition	$\Gamma^{hydrated}_{HA-\beta-CD}$, ng/cm^2	Detached under E_{ox}
Direct SAM formation	SAM Fc^{C11}	538 ± 38	85 ± 6 %
SAM post-functionalization	SAM^{click} Fc^{C11}	410 ± 30	18 ± 2 %

Fig. 7. Dependence of β-CD/Fc interactions on the Fc grafting method. (A-B) Schematic of HA-β-CD binding to SAM Fc^{C11} (A) and SAM^{click} Fc^{C11} (B) with representative Δf (blue) and ΔD (red) shifts recorded upon HA-β-CD injection and rinsing accompanied by E_{ox} application; E_{ox} application was stopped once signal is stabilized. **(C)** Studied SAM compositions with corresponding masses of hydrated HA-β-CD films, $\Gamma^{hydrated}_{HA-\beta-CD}$ and fraction of the detached HA-β-CD, determined as described in Fig. 6. **Conditions**: Γ_{Fc} = 335-455 pmol/cm^2, electrolyte = 0.1 M KPF$_6$, E_{ox} = 0.45 V, $c_{HA-\beta-CD}$ = 50 μg/mL (1.9 μM of polymer chains), flow = 20 μL/min. The solutions in contact with the surfaces at different moments of time are indicated on the top of QCM-D profiles. Black arrows indicate the moments of applying E_{ox}.

In the second set of experiments, we fixed the Fc linker to the rigid C11 chain and studied the role of Fc grafting method on the β-CD/Fc interactions. For this, Fc SAMs obtained *via* direct formation were compared to Fc SAMs obtained through post-functionalization. The two cases were studied in the absence of diluting thiols, i.e. at maximal Fc surface density Γ_{Fc} = 335-455 pmol/cm^2, which corresponds to the average distance between Fc moieties l_{Fc} = 0.6 - 0.7 nm (assuming square lattice). The characteristic E-QCM-D profiles are shown in Fig. 7A for SAM Fc^{C11}, obtained by direct self-assembly of SH-(CH$_2$)$_{11}$-Fc, and in Fig. 7B for SAM^{click} Fc^{C11}, obtained by self-assembly of SH-(CH$_2$)$_{11}$-N$_3$ followed by click reaction with Fc alkyne, as schematically shown in Fig. 2A. Fig. 7C summarizes $\Gamma^{hydrated}_{HA-\beta-CD}$ and fraction of detached HA-β-CD determined by viscoelastic modeling.

Interestingly, the oxidation of the directly generated SAM Fc^{C11} resulted in quasi-complete detachment of the bound HA-β-CD (Fig. 7A), in contrast to the modest detachment observed for the post-functionalized Fc SAMs (Fig. 7B, Figs. 5, 6). As discussed in the Section 3.1.1, the main feature of the directly generated Fc SAMs as compared to those obtained by post-functionalization is their heterogeneity, including regions with clustered Fc molecules, facilitated by the interchain interaction of Fc thiols.[40,41,62] The random orientation of Fc moieties (i.e. hidden in monolayer or exposed to solution) together with the increased steric hindrance inside the clusters should reduce the number of formed β-CD/Fc bonds per HA-β-CD, resulting in more loosely attached HA-β-CD chains forming more extended HA-β-CD coating (reflected by higher QCM-D signal), thus facilitating its detachment (Fig. 7A). Besides, in the case of directly formed SAM Fc^{C11}, the presence of Fc clusters was shown to induce an increase in the positive charge around Fc moieties during oxidation, accompanied by the anodic shift of $E^{0'}$.[40] This local positive charge around β-CD moieties may additionally facilitate the disassembly of β-CD/Fc$^+$ complexes, despite a certain global electrostatic attraction that may occur between Fc$^+$ SAMs and negatively charged HA backbone.

The obtained E-QCM-D results show that surface chemistry strongly influences both host/guest binding and redox-driven dissociation and that the organization of guest SAMs and flexibility of guest linkers are among the main parameters which determine the efficiency of these two processes.

3.3. Summary of the obtained findings

Our main findings are schematically shown in Fig. 8 and can be summarized as follows:

(i) The efficiency of SAM post-functionalization depends on the nature of the linkers connecting active groups to the surface and can be optimized by adjusting their flexibility (Figure 8A).

(ii) The 2D organization of guest SAMs can be improved by using two-step post-functionalization instead of direct grafting, and their repellent properties can be optimized using hydrophilic diluting molecules (Figure 8B).

(iii) The efficiency of host/guest assembly and detachment depends on the availability of guest moieties on the surface, which is determined by the organization of guest SAMs and by the flexibility of guest linkers (Figure 8C).

Point (i) requires proper consideration to ensure interface functionality when modifying SAMs *via* click chemistry. Among the studied systems, the mixed alkyl/EG-N$_3$ linker provides the highest conversion efficiency of azides to triazoles, a fact we attribute to a combination of sufficient density, accessibility, and flexibility of the azide end groups at the top of the SAM. While the EG end groups provide flexibility, the rigid alkyl chains ensure good organization and high density of the SAM and consequently favor the orientation of azide groups towards click solution.

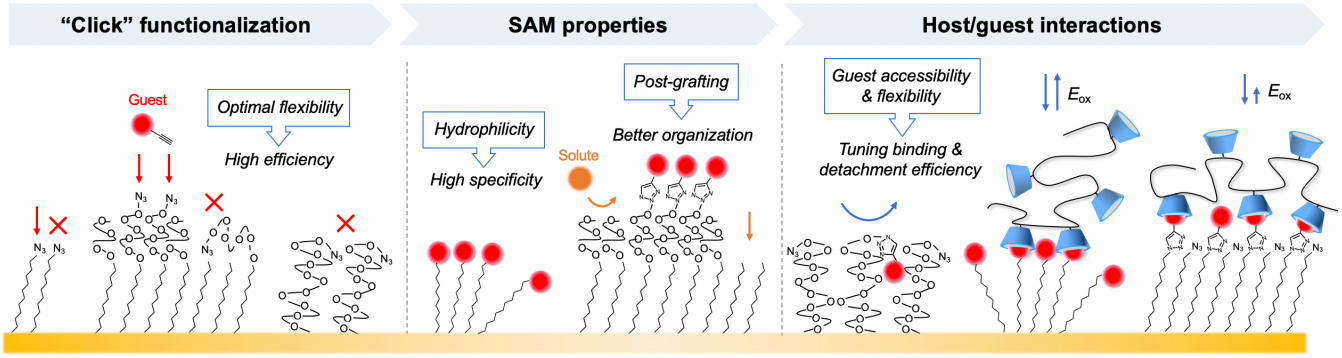

Fig. 8. Summary of the obtained findings. Schematic representation of the effects of surface chemistry on the click-functionalization efficiency **(A)**, the properties of guest SAMs **(B)** and the resulting host/guest interactions **(C)**.

Special attention should also be given to the choice of diluting molecules in mixed monolayers as this can affect the efficiency of SAM functionalization (i) and their repellent properties (ii). Mixed alkyl/EG diluting thiol appears optimal as it provides good SAM organization due to the presence of alkyl chains (compared to EG chain alone), orientation of functional groups towards solution, which increases efficiency of SAM post-functionalization (in the case of mixed alkyl/EG guest linkers, Fig. 8A), and suppression of non-specific binding due to the repellent properties of EG (compared to alkyl chain alone, Fig. 8B). Another important aspect to consider is the correlation between the method of SAM formation and the 2D organization of guest moieties (ii). Our data show that the two-step post-functionalization method improves the homogeneity of guest presentation in the monolayer as compared to direct grafting. We hypothesize that this is due to the fact that click grafting only takes place at the azide groups exposed to the solution phase. Besides, post-functionalization allows to improve the reproducibility of SAM characteristics, including guest density (Fig. 2C) and the shape of the redox signatures (Fig. S5).

Furthermore, this study reveals several important correlations between the formation of guest SAMs (i, ii) and the resulting host/guest interactions (iii). Thus, SAMs formed using alkyl or mixed alkyl/OEG linkers appear to be optimal for efficient host/guest complexation, which we attribute to their high density and good organization, ensuring that the guest groups are oriented towards the solution side. Much weaker guest accessibility is expected in the case of less organized and more flexible SAMs composed of pure OEG linkers, which we believe explains the lack of host/guest binding (Fig. 8C). In addition to the impaired accessibility of guest molecules, the high flexibility of OEG chains must induce larger conformational changes required for HA-β-CD fixation, thereby increasing the entropic cost at such interfaces. A similar trend was observed when studying the effect of the linker connecting the HA backbone to β-CD groups: its suppression led to an increase in HA-β-CD binding over a large range of guest surface densities.[17]

Another interesting correlation concerns the higher detachment efficiency of host molecules from directly formed SAMs as compared to post-functionalized SAMs. We attribute this to the poor organization of guests in directly formed SAMs, which leads to a lower effective density of guests on the surface and, consequently, to a lower number of formed host/guest bonds (Fig. 8C). This interpretation is in line with weaker QCM-D signals upon HA-β-CD binding and less efficient HA-β-CD detachment at higher Fc surface density, when comparing diluted SAM^{click} Fc^{C11}-CH_3^{C10} (Γ_{Fc} = 59 pmol/cm^2, Fig. 6B) with saturated SAM^{click} Fc^{C11} (Γ_{Fc} = 350 pmol/cm^2, Fig. 7B). In addition, control experiments on highly diluted Fc SAMs ($\Gamma_{Fc} \leq$ 10 pmol/cm^2) showed that limiting the number of β-CD/Fc bonds indeed allows complete detachment of HA-β-CD (Fig. S6), confirming the crucial role of this parameter in multivalent systems.[46] Besides, the slow gradual changes in QCM-D signals upon oxidation observed for the post-functionalized Fc SAMs (Fig. 6) suggest that polymer reorganization/release may take considerable time when it is attached to the surface through many β-CD/Fc bonds, thus indicating the presence of kinetic limitations in these dynamic systems.

These findings suggest that rational design of stimuli-responsive interfaces requires considering not only the average density of host/guest moieties, but also their accessibility and conformational flexibility on the surface, together with the chemical nature of surrounding molecules. The repellent properties of hydrophilic linkers and diluents should also be considered, since the specificity of host/guest interactions is one of the factors determining the successful design of stimuli-responsive host/guest interfaces.

CONCLUSIONS

We have performed a systematic study involving electrochemical, QCM-D and contact angle characterization to understand how surface chemistry affects the formation of guest monolayers and their subsequent interactions with soluble host probes. Using β-CD/Fc pair as a model system, we have demonstrated that surface density, homogeneity and repellent properties of Fc monolayers are essentially governed by the method of monolayer formation (direct assembly *vs* post-functionalization) and the nature of chosen linkers and diluting molecules (i.e., flexibility, hydrophilicity). In particular, mixed alkyl/OEG monolayers are preferred over rigid alkyl chains because of their ability to suppress non-specific interactions and enhance post-functionalization efficiency, with quantitative azide/alkyne click conversion achieved for diluted alkyl/OEG SAMs. At the same time, the accessibility of azides was impaired in monolayers composed of pure PEG chains, indicating a subtle relationship between linker flexibility and post-functionalization efficiency. Finally, strong correlations have been

identified between the 2D organization and flexibility of guest monolayers and the efficiency and reversibility of host/guest complexation. Our results show that successful binding and detachment of host probes is influenced not only by the density of surface guests, as previously reported,[46] but also by their conformational flexibility and accessibility, which in turn are determined by the choice of grafting method and the nature of molecular linkers and diluents.

The obtained findings should be applicable to different host/guest interactions, including photo- or redox-sensitive complexes between β-CD and other guests (e.g. azobenzene),[49,51,52,54] Fc and other hosts (e.g., cucurbit[7]uril),[6,28] and other host/guest pairs (e.g. cucurbit[8]uril/viologen, pillar[n]arene complexes),[3,6,7] and thus promote the development of well-defined functional interfaces for numerous applications in sensing,[13,28] catalysis,[3,11] material sciences[2,3,6,7,14,44] and biomedicine.[15,34,52,54] Besides, the obtained knowledge about the interplay between surface chemistry, monolayer organization and supramolecular interactions can be applied to other ligand/receptor pairs and thus contributes to the general understanding of self-assembly and multivalent interactions at functional interfaces,[8,9,46,47] facilitating their progressive use in material and biochemical sciences.

ASSOCIATED CONTENT

Supporting Information

The Supporting Information, which includes AFM characterization of gold surfaces, QCM-D characterization of repelling properties, E-QCM-D monitoring of host/guest binding to diluted monolayers and additional contact angle and electrochemical data, is available free of charge on the ACS Publications website.

AUTHOR INFORMATION

Corresponding Author

*Galina V. Dubacheva – Department of Molecular Chemistry, Université Grenoble Alpes, CNRS UMR 5250, Grenoble 38000, France; orcid.org/0000-0003-1417-5381; Email: galina.dubacheva@univ-grenoble-alpes.fr.

Author Contributions

The manuscript was written through contributions of all authors. All authors have given approval to the final version of the manuscript.

Notes

The authors declare no competing financial interest.

ACKNOWLEDGMENT

This work was supported by ANR JCJC "SupraSwitch" funding (ANR-18-CE09-0009). The authors also acknowledge ICMG FR2607 Chemistry Nanobio Platform (DCM, UGA) and support from LabEx ARCANE and CBH-EUR-GS (ANR-17-EURE-0003). Arielle Le Pellec (DCM, UGA) is acknowledged for help with metal surface coatings.

REFERENCES

(1) Teyssandier, J.; Feyter, S. D.; Mali, K. S. Host–Guest Chemistry in Two-Dimensional Supramolecular Networks. *Chem. Commun.* **2016**, *52* (77), 11465–11487. https://doi.org/10.1039/C6CC05256H.

(2) Ludden, M. J. W.; Reinhoudt, D. N.; Huskens, J. Molecular Printboards: Versatile Platforms for the Creation and Positioning of Supramolecular Assemblies and Materials. *Chem. Soc. Rev.* **2006**, *35* (11), 1122–1134. https://doi.org/10.1039/B600093M.

(3) Yang, H.; Yuan, B.; Zhang, X.; Scherman, O. A. Supramolecular Chemistry at Interfaces: Host–Guest Interactions for Fabricating Multifunctional Biointerfaces. *Acc. Chem. Res.* **2014**, *47* (7), 2106–2115. https://doi.org/10.1021/ar500105t.

(4) Yang, Y.-W.; Sun, Y.-L.; Song, N. Switchable Host–Guest Systems on Surfaces. *Acc. Chem. Res.* **2014**, *47* (7), 1950–1960. https://doi.org/10.1021/ar500022f.

(5) Zhan, W.; Wei, T.; Yu, Q.; Chen, H. Fabrication of Supramolecular Bioactive Surfaces via β-Cyclodextrin-Based Host–Guest Interactions. *ACS Appl. Mater. Interfaces* **2018**, *10* (43), 36585–36601. https://doi.org/10.1021/acsami.8b12130.

(6) Wiemann, M.; Jonkheijm, P. Stimuli-Responsive Cucurbit[n]Uril-Mediated Host-Guest Complexes on Surfaces. *Isr. J. Chem.* **2018**, *58* (3–4), 314–325. https://doi.org/10.1002/ijch.201700109.

(7) Lou, X.-Y.; Yang, Y.-W. Pillar[n]Arene-Based Supramolecular Switches in Solution and on Surfaces. *Adv. Mater.* **2020**, *32* (43), 2003263. https://doi.org/10.1002/adma.202003263.

(8) Fasting, C.; Schalley, C. A.; Weber, M.; Seitz, O.; Hecht, S.; Koksch, B.; Dernedde, J.; Graf, C.; Knapp, E.-W.; Haag, R. Multivalency as a Chemical Organization and Action Principle. *Angew. Chem. Int. Ed.* **2012**, *51* (42), 10472–10498. https://doi.org/10.1002/anie.201201114.

(9) Varner, C. T.; Rosen, T.; Martin, J. T.; Kane, R. S. Recent Advances in Engineering Polyvalent Biological Interactions. *Biomacromolecules* **2015**, *16* (1), 43–55. https://doi.org/10.1021/bm5014469.

(10) Di Iorio, D.; Huskens, J. Surface Modification with Control over Ligand Density for the Study of Multivalent Biological Systems. *ChemistryOpen* **2020**, *9* (1), 53–66. https://doi.org/10.1002/open.201900290.

(11) Wan, P.; Chen, X. Stimuli-Responsive Supramolecular Interfaces for Controllable Bioelectrocatalysis. *ChemElectroChem* **2014**, *1* (10), 1602–1612. https://doi.org/10.1002/celc.201402266.

(12) Ashwin, B. C. M. A.; Shanmugavelan, P.; Muthu Mareeswaran, P. Electrochemical Aspects of Cyclodextrin, Calixarene and Cucurbituril Inclusion Complexes. *J. Incl. Phenom. Macrocycl. Chem.* **2020**, *98* (3), 149–170. https://doi.org/10.1007/s10847-020-01028-4.

(13) d'Astous, É. V.; Dauphin-Ducharme, P. Harnessing Host–Guest Chemistry for Electrochemical Sensing in Complex Matrices. *Curr. Opin. Electrochem.* **2022**, *34*, 101029. https://doi.org/10.1016/j.coelec.2022.101029.

(14) Quan, J.; Guo, Y.; Ma, J.; Long, D.; Wang, J.; Zhang, L.; Sun, Y.; Dhinakaran, M. K.; Li, H. Light-Responsive Nanochannels Based on the Supramolecular Host–Guest System. *Front. Chem.* **2022**, *10*.

(15) Degardin, M.; Thakar, D.; Claron, M.; Richter, R. P.; Coche-Guérente, L.; Boturyn, D. Development of a Selective Cell Capture and Release Assay: Impact of Clustered RGD Ligands. *J. Mater. Chem. B* **2017**, *5* (24), 4745–4753. https://doi.org/10.1039/C7TB00630F.

(16) Dubacheva, G. V.; Curk, T.; Mognetti, B. M.; Auzély-Velty, R.; Frenkel, D.; Richter, R. P. Superselective Targeting Using Multivalent Polymers. *J. Am. Chem. Soc.* **2014**, *136* (5), 1722–1725. https://doi.org/10.1021/ja411138s.

(17) Dubacheva, G. V.; Curk, T.; Auzély-Velty, R.; Frenkel, D.; Richter, R. P. Designing Multivalent Probes for Tunable Superselective Targeting. *Proc. Natl. Acad. Sci.* **2015**, *112* (18), 5579–5584. https://doi.org/10.1073/pnas.1500622112.

(18) Ju, H.; Leech, D. Host–Guest Interaction at a Self-Assembled Monolayer/Solution Interface: An Electrochemical Analysis of the Inclusion of 11-(Ferrocenylcarbonyloxy)Undecanethiol by Cyclodextrins. *Langmuir* **1998**, *14* (2), 300–306. https://doi.org/10.1021/la970356x.

(19) Park, J.; Park, J.; Lee, J.; Lim, C.; Lee, D. W. Size Compatibility and Concentration Dependent Supramolecular Host–Guest Interactions at Interfaces. *Nat. Commun.* **2022**, *13* (1), 112. https://doi.org/10.1038/s41467-021-27659-w.

(20) Sankaran, S.; Cavatorta, E.; Huskens, J.; Jonkheijm, P. Cell Adhesion on RGD-Displaying Knottins with Varying Numbers of Tryptophan Amino Acids to Tune the Affinity for Assembly on Cucurbit[8]Uril Surfaces. *Langmuir* **2017**, *33* (35), 8813–8820. https://doi.org/10.1021/acs.langmuir.7b00702.

(21) Sankaran, S.; de Ruiter, M.; Cornelissen, J. J. L. M.; Jonkheijm, P. Supramolecular Surface Immobilization of Knottin Derivatives for Dynamic Display of High Affinity Binders. *Bioconjug. Chem.* **2015**, *26* (9), 1972–1980. https://doi.org/10.1021/acs.bioconjchem.5b00419.

(22) Yang, L.; Gomez-Casado, A.; Young, J. F.; Nguyen, H. D.; Cabanas-Danés, J.; Huskens, J.; Brunsveld, L.; Jonkheijm, P. Reversible and Oriented Immobilization of Ferrocene-Modified Proteins. *J. Am. Chem. Soc.* **2012**, *134* (46), 19199–19206. https://doi.org/10.1021/ja308450n.

(23) Bacharouche, J.; Degardin, M.; Jierry, L.; Carteret, C.; Lavalle, P.; Hemmerlé, J.; Senger, B.; Auzély-Velty, R.; Boulmedais, F.; Boturyn, D.; Coche-Guérente, L.; Schaaf, P.; Francius, G. Multivalency: Influence of the Residence Time and the Retraction Rate on Rupture Forces Measured by AFM. *J. Mater. Chem. B* **2015**, *3* (9), 1801–1812. https://doi.org/10.1039/C4TB01261E.

(24) Nijhuis, C. A.; Huskens, J.; Reinhoudt, D. N. Binding Control and Stoichiometry of Ferrocenyl Dendrimers at a Molecular Printboard. *J. Am. Chem. Soc.* **2004**, *126* (39), 12266–12267. https://doi.org/10.1021/ja048271n.

(25) Sanchez Perez, E.; Toor, R.; Bruyat, P.; Cepeda, C.; Degardin, M.; Dejeu, J.; Boturyn, D.; Coche-Guérente, L. Impact of Multimeric Ferrocene-Containing Cyclodecapeptide Scaffold on Host-Guest Interactions at a β-Cyclodextrin Covered Surface. *ChemPhysChem* **2021**, *22* (21), 2231–2239. https://doi.org/10.1002/cphc.202100469.

(26) Dubacheva, G. V.; Curk, T.; Frenkel, D.; Richter, R. P. Multivalent Recognition at Fluid Surfaces: The Interplay of Receptor Clustering and Superselectivity. *J. Am. Chem. Soc.* **2019**, *141* (6), 2577–2588. https://doi.org/10.1021/jacs.8b12553.

(27) Rojas, M. T.; Koeniger, R.; Stoddart, J. F.; Kaifer, A. E. Supported Monolayers Containing Preformed Binding Sites. Synthesis and Interfacial Binding Properties of a Thiolated .Beta.-Cyclodextrin Derivative. *J. Am. Chem. Soc.* **1995**, *117* (1), 336–343. https://doi.org/10.1021/ja00106a036.

(28) Qi, L.; Wang, R.; Yu, H.-Z. Electrochemical Quantitation of Supramolecular Excipient@Drug Complexation: A General Assay Strategy Based on Competitive Host Binding with Surface-Immobilized Redox Guest. *Anal. Chem.* **2020**, *92* (2), 2168–2175. https://doi.org/10.1021/acs.analchem.9b04803.

(29) Domi, Y.; Ikeura, K.; Okamura, K.; Shimazu, K.; Porter, M. D. Strong Inclusion of Inorganic Anions into β-Cyclodextrin Immobilized to Gold Electrode. *Langmuir* **2011**, *27* (17), 10580–10586. https://doi.org/10.1021/la1051063.

(30) Veerbeek, J.; Méndez-Ardoy, A.; Huskens, J. Electrochemistry of Redox-Active Guest Molecules at β-Cyclodextrin-Functionalized Silicon Electrodes. *ChemElectroChem* **2017**, *4* (6), 1470–1477. https://doi.org/10.1002/celc.201600872.

(31) Qi, L.; Tian, H.; Shao, H.; Yu, H.-Z. Host–Guest Interaction at Molecular Interfaces: Cucurbit[7]Uril as a Sensitive Probe of Structural Heterogeneity in Ferrocenyl Self-Assembled Monolayers on Gold. *J. Phys. Chem. C* **2018**, *122* (28), 15986–15995. https://doi.org/10.1021/acs.jpcc.8b01067.

(32) Coutouli-Argyropoulou, E.; Kelaidopoulou, A.; Sideris, C.; Kokkinidis, G. Electrochemical Studies of Ferrocene Derivatives and Their Complexation by β-Cyclodextrin. *J. Electroanal. Chem.* **1999**, *477* (2), 130–139. https://doi.org/10.1016/S0022-0728(99)00397-6.

(33) Khan, A.; Wang, L.; Yu, H.; Haroon, M.; Ullah, R. S.; Nazir, A.; Elshaarani, T.; Usman, M.; Fahad, S.; Haq, F. Research Advances in the Synthesis and Applications of Ferrocene-Based Electro and Photo Responsive Materials. *Appl. Organomet. Chem.* **2018**, *32* (12), e4575. https://doi.org/10.1002/aoc.4575.

(34) Gao, T.; Li, L.; Wang, B.; Zhi, J.; Xiang, Y.; Li, G. Dynamic Electrochemical Control of Cell Capture-and-Release Based on Redox-Controlled Host–Guest Interactions. *Anal. Chem.* **2016**, *88* (20), 9996–10001. https://doi.org/10.1021/acs.analchem.6b02156.

(35) Dubacheva, G. V.; Van der Heyden, A.; Dumy, P.; Kaftan, O.; Auzély-Velty, R.; Coche-Guerente, L.; Labbé, P. Electrochemically Controlled Adsorption of Fc-Functionalized Polymers on Beta-CD-Modified Self-Assembled Monolayers. *Langmuir ACS J. Surf. Colloids* **2010**, *26* (17), 13976–13986. https://doi.org/10.1021/la102026h.

(36) Liang, C.-K.; Dubacheva, G. V.; Buffeteau, T.; Cavagnat, D.; Hapiot, P.; Fabre, B.; Tucker, J. H. R.; Bassani, D. M. Reversible Control over Molecular Recognition in Surface-Bound Photoswitchable Hydrogen-Bonding Receptors: Towards Read–Write–Erase Molecular Printboards. *Chem. – Eur. J.* **2013**, *19* (38), 12748–12758. https://doi.org/10.1002/chem.201301613.

(37) Collman, J. P.; Devaraj, N. K.; Chidsey, C. E. D. "Clicking" Functionality onto Electrode Surfaces. *Langmuir* **2004**, *20* (4), 1051–1053. https://doi.org/10.1021/la0362977.

(38) Collman, J. P.; Devaraj, N. K.; Eberspacher, T. P. A.; Chidsey, C. E. D. Mixed Azide-Terminated Monolayers: A Platform for Modifying Electrode Surfaces. *Langmuir* **2006**, *22* (6), 2457–2464. https://doi.org/10.1021/la052947q.

(39) Fabre, B. Ferrocene-Terminated Monolayers Covalently Bound to Hydrogen-Terminated Silicon Surfaces. Toward the Development of Charge Storage and Communication Devices. *Acc. Chem. Res.* **2010**, *43* (12), 1509–1518. https://doi.org/10.1021/ar100085q.

(40) Lee, L. Y. S.; Sutherland, T. C.; Rucareanu, S.; Lennox, R. B. Ferrocenylalkylthiolates as a Probe of Heterogeneity in Binary Self-Assembled Monolayers on Gold. *Langmuir* **2006**, *22* (9), 4438–4444. https://doi.org/10.1021/la053317r.

(41) Auletta, T.; van Veggel, F. C. J. M.; Reinhoudt, D. N. Self-

Assembled Monolayers on Gold of Ferrocene-Terminated Thiols and Hydroxyalkanethiols. *Langmuir* **2002**, *18* (4), 1288–1293. https://doi.org/10.1021/la011474u.

(42) Dubacheva, G. V.; Galibert, M.; Coche-Guerente, L.; Dumy, P.; Boturyn, D.; Labbé, P. Redox Strategy for Reversible Attachment of Biomolecules Using Bifunctional Linkers. *Chem. Commun.* **2011**, *47* (12), 3565–3567. https://doi.org/10.1039/C0CC05647B.

(43) Thakar, D.; Coche-Guérente, L.; Claron, M.; Wenk, C. H. F.; Dejeu, J.; Dumy, P.; Labbé, P.; Boturyn, D. Redox-Driven Host–Guest Interactions Allow the Controlled Release of Captured Cells on RGD-Functionalized Surfaces. *ChemBioChem* **2014**, *15* (3), 377–381. https://doi.org/10.1002/cbic.201300636.

(44) Ling, X. Y.; Reinhoudt, D. N.; Huskens, J. Reversible Attachment of Nanostructures at Molecular Printboards through Supramolecular Glue. *Chem. Mater.* **2008**, *20* (11), 3574–3578. https://doi.org/10.1021/cm703597w.

(45) Dubacheva, G. V.; Dumy, P.; Auzély, R.; Schaaf, P.; Boulmedais, F.; Jierry, L.; Coche-Guerente, L.; Labbé, P. Unlimited Growth of Host–Guest Multilayer Films Based on Functionalized Neutral Polymers. *Soft Matter* **2010**, *6* (16), 3747–3750. https://doi.org/10.1039/C0SM00324G.

(46) Dubacheva, G. V.; Curk, T.; Richter, R. P. Determinants of Superselectivity—Practical Concepts for Application in Biology and Medicine. *Acc. Chem. Res.* **2023**, *56* (7), 729–739. https://doi.org/10.1021/acs.accounts.2c00672.

(47) Mulder, A.; Huskens, J.; N. Reinhoudt, D. Multivalency in Supramolecular Chemistry and Nanofabrication. *Org. Biomol. Chem.* **2004**, *2* (23), 3409–3424. https://doi.org/10.1039/B413971B.

(48) Zhang, X.; Ma, X.; Wang, K.; Lin, S.; Zhu, S.; Dai, Y.; Xia, F. Recent Advances in Cyclodextrin-Based Light-Responsive Supramolecular Systems. *Macromol. Rapid Commun.* **2018**, *39* (11), 1800142. https://doi.org/10.1002/marc.201800142.

(49) Zhang, Y.; Ren, L.; Tu, Q.; Wang, X.; Liu, R.; Li, L.; Wang, J.-C.; Liu, W.; Xu, J.; Wang, J. Fabrication of Reversible Poly(Dimethylsiloxane) Surfaces via Host–Guest Chemistry and Their Repeated Utilization in Cardiac Biomarker Analysis. *Anal. Chem.* **2011**, *83* (24), 9651–9659. https://doi.org/10.1021/ac202517x.

(50) Ni, Y.; Zhang, D.; Wang, Y.; He, X.; He, J.; Wu, H.; Yuan, J.; Sha, D.; Che, L.; Tan, J.; Yang, J. Host–Guest Interaction-Mediated Photo/Temperature Dual-Controlled Antibacterial Surfaces. *ACS Appl. Mater. Interfaces* **2021**, *13* (12), 14543–14551. https://doi.org/10.1021/acsami.0c21626.

(51) Deng, J.; Liu, X.; Shi, W.; Cheng, C.; He, C.; Zhao, C. Light-Triggered Switching of Reversible and Alterable Biofunctionality via β-Cyclodextrin/Azobenzene-Based Host-Guest Interaction. *ACS Macro Lett.* **2014**, *3* (11), 1130–1133. https://doi.org/10.1021/mz500568k.

(52) Bian, Q.; Wang, W.; Wang, S.; Wang, G. Light-Triggered Specific Cancer Cell Release from Cyclodextrin/Azobenzene and Aptamer-Modified Substrate. *ACS Appl. Mater. Interfaces* **2016**, *8* (40), 27360–27367. https://doi.org/10.1021/acsami.6b09734.

(53) Gong, Y.-H.; Li, C.; Yang, J.; Wang, H.-Y.; Zhuo, R.-X.; Zhang, X.-Z. Photoresponsive "Smart Template" via Host–Guest Interaction for Reversible Cell Adhesion. *Macromolecules* **2011**, *44* (19), 7499–7502. https://doi.org/10.1021/ma201676w.

(54) Shi, P.; Ju, E.; Wang, J.; Yan, Z.; Ren, J.; Qu, X. Host–Guest Recognition on Photo-Responsive Cell Surfaces Directs Cell–Cell Contacts. *Mater. Today* **2017**, *20* (1), 16–21. https://doi.org/10.1016/j.mattod.2016.12.006.

(55) Rekharsky, M. V.; Inoue, Y. Complexation Thermodynamics of Cyclodextrins. *Chem. Rev.* **1998**, *98* (5), 1875–1918. https://doi.org/10.1021/cr970015o.

(56) Méndez-Ardoy, A.; Steentjes, T.; Boukamp, B. A.; Jonkheijm, P.; Kudernac, T.; Huskens, J. Electron-Transfer Rates in Host–Guest Assemblies at β-Cyclodextrin Monolayers. *Langmuir* **2017**, *33* (35), 8614–8623. https://doi.org/10.1021/acs.langmuir.6b03860.

(57) Beulen, M. W. J.; Bügler, J.; Lammerink, B.; Geurts, F. A. J.; Biemond, E. M. E. F.; van Leerdam, K. G. C.; van Veggel, F. C. J. M.; Engbersen, J. F. J.; Reinhoudt, D. N. Self-Assembled Monolayers of Heptapodant β-Cyclodextrins on Gold. *Langmuir* **1998**, *14* (22), 6424–6429. https://doi.org/10.1021/la980936+.

(58) Endo, H.; Nakaji-Hirabayashi, T.; Morokoshi, S.; Gemmei-Ide, M.; Kitano, H. Orientational Effect of Surface-Confined Cyclodextrin on the Inclusion of Bisphenols. *Langmuir* **2005**, *21* (4), 1314–1321. https://doi.org/10.1021/la048595p.

(59) Nelles, G.; Weisser, M.; Back, R.; Wohlfart, P.; Wenz, G.; Mittler-Neher, S. Controlled Orientation of Cyclodextrin Derivatives Immobilized on Gold Surfaces. *J. Am. Chem. Soc.* **1996**, *118* (21), 5039–5046. https://doi.org/10.1021/ja9539812.

(60) Steentjes, T.; Jonkheijm, P.; Huskens, J. Electron Transfer Processes in Ferrocene-Modified Poly(Ethylene Glycol) Monolayers on Electrodes. *Langmuir* **2017**, *33* (43), 11878–11883. https://doi.org/10.1021/acs.langmuir.7b02160.

(61) Rudnev, A. V.; Zhumaev, U.; Utsunomiya, T.; Fan, C.; Yokota, Y.; Fukui, K.; Wandlowski, T. Ferrocene-Terminated Alkanethiol Self-Assembled Monolayers: An Electrochemical and in Situ Surface-Enhanced Infra-Red Absorption Spectroscopy Study. *Electrochimica Acta* **2013**, *107*, 33–44. https://doi.org/10.1016/j.electacta.2013.05.134.

(62) Tian, H.; Dai, Y.; Shao, H.; Yu, H.-Z. Modulated Intermolecular Interactions in Ferrocenylalkanethiolate Self-Assembled Monolayers on Gold. *J. Phys. Chem. C* **2013**, *117* (2), 1006–1012. https://doi.org/10.1021/jp310012v.

(63) Tian, H.; Qi, L.; Xiang, D.; Shao, H.; Yu, H.-Z. Homogenized Redox Behavior of Electroactive Self-Assembled Monolayers on Gold in the Organic Phase. *Electrochimica Acta* **2015**, *170*, 369–375. https://doi.org/10.1016/j.electacta.2015.04.143.

(64) Valincius, G.; Niaura, G.; Kazakevičienė, B.; Talaikytė, Z.; Kažemėkaitė, M.; Butkus, E.; Razumas, V. Anion Effect on Mediated Electron Transfer through Ferrocene-Terminated Self-Assembled Monolayers. *Langmuir* **2004**, *20* (16), 6631–6638. https://doi.org/10.1021/la0364800.

(65) Smalley, J. F.; Feldberg, S. W.; Chidsey, C. E. D.; Linford, M. R.; Newton, M. D.; Liu, Y.-P. The Kinetics of Electron Transfer Through Ferrocene-Terminated Alkanethiol Monolayers on Gold. *J. Phys. Chem.* **1995**, *99* (35), 13141–13149. https://doi.org/10.1021/j100035a016.

(66) Amatore, C.; Maisonhaute, E.; Schöllhorn, B.; Wadhawan, J. Ultrafast Voltammetry for Probing Interfacial Electron Transfer in Molecular Wires. *ChemPhysChem* **2007**, *8* (9), 1321–1329. https://doi.org/10.1002/cphc.200600774.

(67) Sabapathy, R. C.; Bhattacharyya, S.; Cleland, W. E.; Hussey, C. L. Host–Guest Complexation in Self-Assembled Monolayers: Inclusion of a Monolayer-Anchored Cationic Ferrocene-Based Guest by Cyclodextrin Hosts. *Langmuir* **1998**, *14* (14), 3797–3807. https://doi.org/10.1021/la960660a.

(68) Bock, V. D.; Hiemstra, H.; van Maarseveen, J. H. CuI-Catalyzed Alkyne–Azide "Click" Cycloadditions from a Mechanistic and Synthetic Perspective. *Eur. J. Org. Chem.* **2006**, *2006* (1), 51–68. https://doi.org/10.1002/ejoc.200500483.

(69) Eisele, N. B.; Andersson, F. I.; Frey, S.; Richter, R. P. Viscoelasticity of Thin Biomolecular Films: A Case Study on Nucleoporin Phenylalanine-Glycine Repeats Grafted to a Histidine-Tag Capturing QCM-D Sensor. *Biomacromolecules* **2012**, *13* (8), 2322–2332. https://doi.org/10.1021/bm300577s.

(70) Tencer, M.; Nie, H.-Y.; Berini, P. A Contact Angle and ToF-SIMS Study of SAM–Thiol Interactions on Polycrystalline Gold. *Appl. Surf. Sci.* **2011**, *257* (9), 4038–4043. https://doi.org/10.1016/j.apsusc.2010.11.171.

(71) Chidsey, C. E. D.; Bertozzi, C. R.; Putvinski, T. M.; Mujsce, A. M. Coadsorption of Ferrocene-Terminated and Unsubstituted Alkanethiols on Gold: Electroactive Self-Assembled Monolayers. *J. Am. Chem. Soc.* **1990**, *112* (11), 4301–4306. https://doi.org/10.1021/ja00167a028.

(72) Isnin, R.; Salam, C.; Kaifer, A. E. Bimodal Cyclodextrin Complexation of Ferrocene Derivatives Containing N-Alkyl Chains of Varying Length. *J. Org. Chem.* **1991**, *56* (1), 35–41. https://doi.org/10.1021/jo00001a009.

(73) Imonigie, J. A.; Macartney, D. H. The Kinetics of Electron-Transfer Reactions of the [FeCp(CpCH2N(CH3)3]+/2+ Couple in the Presence of Cyclodextrins in Aqueous Media. *Inorganica Chim. Acta* **1994**, *225* (1), 51–56. https://doi.org/10.1016/0020-1693(94)04028-1.

(74) Godínez, L. A.; Schwartz, L.; Criss, C. M.; Kaifer, A. E. Thermodynamic Studies on the Cyclodextrin Complexation of Aromatic and Aliphatic Guests in Water and Water–Urea Mixtures. Experimental Evidence for the Interaction of Urea with Arene Surfaces. *J. Phys. Chem. B* **1997**, *101* (17), 3376–3380. https://doi.org/10.1021/jp970359i.

(75) Godinez, L. A.; Patel, S.; Criss, C. M.; Kaifer, A. E. Calorimetric Studies on the Complexation of Several Ferrocene Derivatives by .Alpha.- and .Beta.-Cyclodextrin. Effects of Urea on the Thermodynamic Parameters. *J. Phys. Chem.* **1995**, *99* (48), 17449–17455. https://doi.org/10.1021/j100048a022.

(76) Ye, S.; Haba, T.; Sato, Y.; Shimazu, K.; Uosaki, K. Coverage Dependent Behavior of Redox Reaction Induced Structure Change and Mass Transport at an 11-Ferrocenyl-1-Undecanethiol Self-Assembled Monolayer on a Gold Electrode Studied by an Insitu IRRAS–EQCM Combined System. *Phys. Chem. Chem. Phys.* **1999**, *1* (15), 3653–3659. https://doi.org/10.1039/A902952D.

Insert Table of Contents artwork here